A&A manuscript no.
(will be inserted by hand later)

Your thesaurus codes are:
20(04.01.1; 04.03.1; 08.08.1; 08.16.3; 10.07.2)

ASTRONOMY AND ASTROPHYSICS

Photometric catalog of nearby globular clusters (I) ⋆

A large homogeneous (V, I) color-magnitude diagram data-base

A. Rosenberg[1], **G. Piotto**[2], **I. Saviane**[2] **and A. Aparicio**[3]

[1] Telescopio Nazionale Galileo, vicolo dell'Osservatorio 5, I–35122 Padova, Italy
[2] Dipartimento di Astronomia, Univ. di Padova, vicolo dell'Osservatorio 5, I–35122 Padova, Italy
[3] Instituto de Astrofisica de Canarias, Via Lactea, E-38200 La Laguna, Tenerife, Spain

Abstract. We present the first part of the first large and homogeneous CCD color-magnitude diagram (CMD) data base, comprising 52 nearby Galactic globular clusters (GGC) imaged in the V and I bands using only two telescopes (one for each hemisphere). The observed clusters represent 75% of the known Galactic globulars with $(m - M)_V \leq 16.15$ mag, cover most of the globular cluster metallicity range ($-2.2 \leq$ [Fe/H] ≤ -0.4), and span Galactocentric distances from ~ 1.2 to ~ 18.5 kpc.

In this paper, the CMDs for the 39 GGCs observed in the southern hemisphere are presented. The remaining 13 northern hemisphere clusters of the catalog are presented in a companion paper. For four clusters (NGC 4833, NGC 5986, NGC 6543, and NGC 6638) we present for the first time a CMD from CCD data. The typical CMD span from the $22^{\rm nd}$ V magnitude to the tip of the red giant branch. Based on a large number of standard stars, the absolute photometric calibration is reliable to the ~ 0.02 mag level in both filters.

This catalog, because of its homogeneity, is expected to represent a useful data base for the measurement of the main absolute and relative parameters characterizing the CMD of GGCs.

Key words: Astronomical data base: miscellaneous - Catalogs - Stars: Hertzsprung-Russel (HR) - Stars: population II - Globular clusters: general

1. Introduction

There are two main properties which make the study of the Galactic globular clusters (GGC) particularly interesting: 1) each cluster (with possible rare exceptions) is made up by a single population of stars, all born at the same time, in the same place, and out of the same material; 2) GGC stars have the oldest measurable age in the Universe, and therefore we believe they are the oldest fossil records of the formation history of our Galaxy.

Among the many tools we have to investigate the properties of a stellar population, the color-magnitude diagrams (CMD) are the most powerful ones, as they allow to recover for each individual star its evolutionary phase, giving precious information on the age of the entire stellar system, its chemical content, and its distance. This information allows us to locate the system in the space, giving a base for the distance scale, study the formation histories of the Galaxy, and test our knowledge of stellar evolution models.

In particular, the study of a large sample of simple stellar systems, as the GGCs, provides important clues to the Milky Way formation history. Recently, many studies on the relative ages of the GGCs have been presented with results at least controversial: while some authors find a notable age spread (~ 5 Gyrs) among the clusters, others find that the bulk of GGCs is coeval. This controversy is surely mainly due to the heterogeneity of the data used in each study, where the combination of photographic and/or CCD data from the early epochs of solid state detectors has been frequently used. For this reason, a survey of both southern and northern GGCs has been started two years ago by means of 1-m class telescopes, i.e. the 91cm European Southern Observatory (ESO) / Dutch telescope and the 1m Isaac Newton Group (ING) / Jacobus Kapteyn telescope (JKT). We were able to collect the data for 52 of the 69 known GGCs with $(m - M)_V \leq 16.15$. Thirty-nine have been observed with the Dutch telescope (data that are presented in this paper, hereafter Paper I), and the remaining ones with the JKT (the corresponding CMDs will be presented in a companion paper, Rosenberg et al. 2000, hereafter Paper II).

As a first exploitation of this new data base, we have conducted a GGC relative age investigation based on the best 34 CMDs of our catalog (Rosenberg et al. 1999, hereafter Paper III), showing that most of the GGCs have the same age. We have also used our data base to obtain a photometric metallicity ranking scale (Saviane et al. 2000, hereafter Paper IV), based on the red giant branch (RGB) morphology. We measured a complete set of metallicity indices, based on the morphology and position of the RGB. Using a grid of selected RGB fiducial points, we defined a function in the $(V - I)_0$, $M_{\rm I}$, [Fe/H] space which is able to reproduce the whole set of GGC RGBs in terms of a single parameter (the metallicity). The use of this

Send offprint requests to: Alfred Rosenberg: alf@iac.es

⋆ Based on data collected at the European Southern Observatory, La Silla, Chile.

function will improve the current determinations of metallicity and distances within the Local Group.

There are many other parameters that can be measured from a homogeneous, well calibrated CMD data base: the horizontal branch (HB) level, homogeneous reddening and distances, etc. We are presently working on these problems. However, we believe it is now the time to present to the community this data base to give to anyone interested the opportunity to take advantage of it.

In the next section, we will describe the observations collected at the ESO/Dutch telescope during two runs in 1997. The data reduction and calibration is presented in Sect. 3, while in Sect. 4 a cross check of the calibration between the two runs is given. In order to facilitate the reader's work, we have included the main parameters characterizing our clusters in Sect. 5. Finally, the observed fields for each cluster, and the obtained CMDs are presented and briefly discussed in Sect. 6.

2. Observations

The data were collected during two runs in 1997: the first in April ($11^{\rm th} - 15^{\rm th}$) and the second in December ($23^{\rm rd}, 24^{\rm th}$ and $26^{\rm th}$). All nights of the first run and the first two of the second run were photometric and had a stable seeing.

Observations were done with the ESO 91cm DUTCH telescope, at La Silla (Chile). The same same CCD#33 was used in both runs, a thinned CCD with 512×512 pixels, each projecting $0.''442$ on the sky, with a total field of view of $3.77 \times 3.77(')^2$, and the same set of V Johnson and i Gunn filters.

Two short ($10-45$s), one medium ($90-120$s) and one long ($600 - 1800$s) exposures were taken in each band (depending on the cluster distance modulus) for one to three fields (in order to ensure a statistically significant sample of stars) for each of the proposed objects. Also a large number of Landolt (1992) standard stars were measured during each night.

In Table 1 the 39 observed GGCs are presented. Column 1 gives an identification number adopted in this paper; cluster NGC numbers and alternative names are given in columns 2 and 3. The observing dates are in column 4, the number of covered fields in column 5, the mean seeing for each filter in column 6, and the integration time for the long exposures in column 7. In Fig. 1 we show the heliocentric distribution of the clusters of our entire catalog.

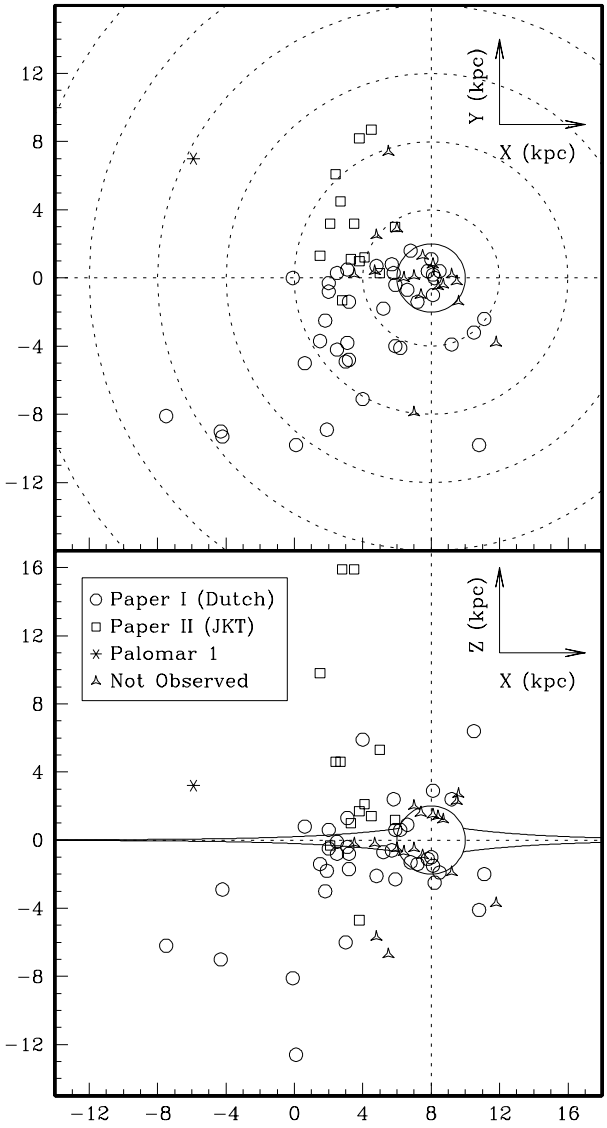

Fig. 1. Heliocentric distribution of all GGCs with $(m-M)_V \leq 16.15$ mag. In the *upper panel*, the GGCs projection over the Galactic plane is presented. The *open circles* represent the clusters studied in the present paper (Paper I); the *open squares*, the GGCs of Paper II; and *the asterisk*, the GGC Pal 1 (Rosenberg et al. 1998). The clusters which are not included in our catalog are marked by *open triangles*. In the *lower panel*, the XZ projection is shown. The Milky Way is schematically represented.

3. Data reduction and calibration

The images were corrected for a constant bias, dark current, and for spatial sensitivity variations using the respective master flats, computed as the median of all available sky flats of the specific run. Afterwards, photometry was performed using the DAOPHOT/ALLSTAR/ALLFRAME software, made available to us by Dr. Stetson (see Stetson 1987, 1994). A preliminary photometry was carried out in order to construct a short list of stars for each single frame. This list was used to accurately match the different frames. With the correct coordinate transformations among the frames, we obtained a single image, median of all the frames, regardless of the filter. In this way we could eliminate all the cosmic rays and obtain the highest signal/noise image for star finding. We ran the DAOPHOT/FIND routine on the median image and performed PSF fitting photometry in order to obtain the deepest list of stellar objects free from spurious detections. Finally, this list was given as input to ALLFRAME, for the simultaneous profile fitting photometry of all the individual frames. We constructed the model PSF for each image using typically from 60 to 120 stars.

Table 1. Observed clusters at the DUTCH in 1997

ID	Cluster (NGC)	Other Name	Obs. date	Obs. fields	Seeing $V/I('')$	Long. Exp.(s)
1	104	47 Tuc	23/Dec	2	1.4/1.3	1800
2	288	-	24/Dec	3	1.4/1.4	1800
3	362	-	26/Dec	3	1.6/1.5	1200
4	1261	-	24/Dec	3	1.3/1.3	1800
5	1851	-	23/Dec	2	1.3/1.2	1800
6	1904	M 79	24/Dec	3	1.3/1.2	1800
7	2298	-	23/Dec	2	1.3/1.2	1800
8	2808	-	11/Apr	2	1.3/1.2	1500
8	2808	-	26/Dec	2	1.5/1.4	1500
9	-	E3	23/Dec	2	1.5/1.4	1800
10	3201	-	12/Apr	2	1.5/1.4	900
10	3201	-	24/Dec	3	1.3/1.2	900
11	4372	-	13/Apr	2	1.3/1.2	1500
12	4590	M 68	14/Apr	2	1.2/1.2	1500
13	4833	-	15/Apr	2	1.3/1.2	1500
14	5139	ω Cen	11/Apr	2	1.2/1.2	900
15	5897	-	12/Apr	1	1.4/1.4	1500
16	5927	-	13/Apr	1	1.3/1.2	1500
17	5986	-	14/Apr	1	1.3/1.3	1500
18	6093	M 80	12/Apr	2	1.3/1.2	1500
19	6101	-	15/Apr	1	1.8/1.7	1500
20	6121	M 4	13/Apr	2	1.3/1.2	900
21	6171	M 107	14/Apr	2	1.4/1.3	1500
22	6266	M 62	14/Apr	1	1.7/1.6	1500
23	6304	-	15/Apr	1	1.5/1.3	1500
24	6352	-	11/Apr	1	1.4/1.3	1500
25	6362	-	12/Apr	1	1.4/1.3	1200
26	6397	-	13/Apr	2	1.3/1.2	900
27	6496	-	14/Apr	1	1.4 1.2	1200
28	6541	-	11/Apr	2	1.3/1.2	1200
29	6544	-	15/Apr	1	1.4/1.4	1500
30	6624	-	12/Apr	1	1.3/1.2	1500
31	6626	M 28	13/Apr	1	1.2/1.1	1500
32	6637	M 69	14/Apr	1	1.2/1.1	1200
33	6638	-	13/Apr	1	1.2/1.2	900
34	6656	M 22	15/Apr	2	1.2/1.2	1500
35	6681	M 70	11/Apr	1	1.3/1.2	1500
36	6717	Pal 9	12/Apr	1	1.3/1.2	1500
37	6723	-	13/Apr	1	1.2/1.1	1200
38	6752	-	14/Apr	1	1.3/1.2	1200
39	6809	M 55	15/Apr	1	1.3/1.1	900

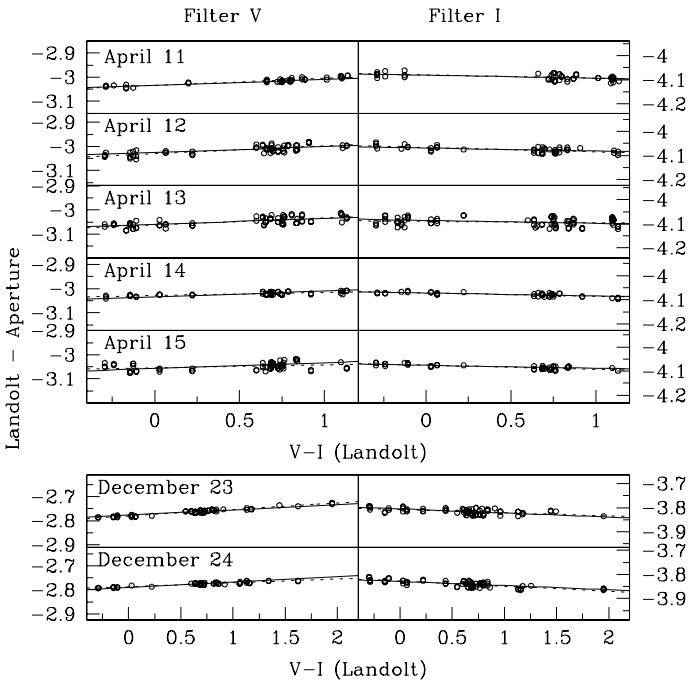

Fig. 2. Calibration equation for each observing night. The *upper panels* refer to the run of April, while the *lower panels* refer to the December run. In all cases, the V filter curves are on the *left side*, while the I filter curves on the right.

Table 2. Calibration parameters for each observing night.

Filter V				
Date	$a_{\rm m}$	error	Cons.	error
11/Apr	+0.024	$\pm$0.001	-3.034	$\pm$0.002
12/Apr	+0.024	$\pm$0.002	-3.025	$\pm$0.004
13/Apr	+0.024	$\pm$0.002	-3.059	$\pm$0.003
14/Apr	+0.024	$\pm$0.001	-3.034	$\pm$0.002
15/Apr	+0.024	$\pm$0.003	-3.057	$\pm$0.004
23/Dec	+0.022	$\pm$0.001	-2.777	$\pm$0.001
24/Dec	+0.022	$\pm$0.001	-2.790	$\pm$0.001
Filter I				
Date	$a_{\rm m}$	error	Cons.	error
11/Apr	-0.012	$\pm$0.003	-4.081	$\pm$0.004
12/Apr	-0.012	$\pm$0.002	-4.069	$\pm$0.003
13/Apr	-0.012	$\pm$0.003	-4.086	$\pm$0.004
14/Apr	-0.012	$\pm$0.001	-4.072	$\pm$0.002
15/Apr	-0.012	$\pm$0.001	-4.076	$\pm$0.004
23/Dec	-0.017	$\pm$0.002	-3.805	$\pm$0.002
24/Dec	-0.017	$\pm$0.002	-3.829	$\pm$0.002

The absolute calibration of the observations to the V-Johnson and I-Cousins systems is based on a set of standard stars from the catalog of Landolt (1992). Specifically, the observed standard stars were in the fields: PG0231, SA95 (41, 43, 96, 97, 98, 100, 101, 102, 112, 115), SA98 (556, 557, 563, 580, 581, L1, 614, 618, 626, 627, 634, 642), RUBIN 149, RUBIN 152, PG0918, PG0942, PG1047, PG1323, PG1525, PG1530, PG1633, and Mark A. At least 3 exposures were taken for each standard field, with a total of $\sim$ 100 standard star measurements per night and per filter.

The reduction and aperture photometry of standard star fields were performed in the same way as for the cluster images. The aperture magnitudes were corrected for atmospheric extinction, assuming $A_V = 0.14$ and $A_I = 0.08$ as extinction coefficients for the V and i filters, respectively.

As shown in Fig. 2, a straight line well reproduces the calibration equations. As the seeing and the overall observing conditions were stable during the run, the slopes of the calibration equations for each observing run and for each filter have been computed using the data from all the nights. As it can be seen in Table 2, the standard deviations of the calibration constants for each run and filter is 0.015mag, corroborating our assumption that all nights were photometric, and that we can assume a constant slope for each filter and run.

Standard stars for which previous problems were reported (PG 1047C, RU149A, RU149G, PG1323A; see Johnson & Bolte 1998) were excluded, as well as saturated stars, those close to a cosmic ray, etc... After this cleaning, the mean slope was computed, and finally the different night constants were found using this slope to fit the individual data, night by night. The adopted values are presented in Table 2. The typical errors (rms) are also given.

The calibration curves are shown in Fig. 2 for both runs. In this figure, the *dotted line* represents the best fitting equation, while the *continuous line* is obtained by best fitting the data imposing the adopted mean slope. The two lines are almost overlapping. The mean number of standard star measures used for computing the curve per night and filter is ~ 75. Notice the wide color coverage for the standard stars.

The last step on the calibration is the aperture correction. As no available bright and isolated stars exist on the cluster images, we used DAOPHOT to subtract from the image the stars in the neighborhood of the brightest ones, in order to compute the difference between the aperture and the PSF-fitting magnitudes. In view of the stable seeing conditions, we used the same aperture for calculating the aperture photometry of the standard and cluster stars.

4. Photometric homogeneity of the two runs

In order to check the photometric homogeneity of the data and of the calibration to the standard photometric system, one cluster (NGC 3201) was observed in both runs. Having one common field, it is possible to analyze the individual star photometry, and test if any additional zero point difference and/or color term exist. The latter check is crucial when measures of the relative position of CMD features are going to be done. The comparison between the two runs is presented in Fig. 3, where 456 common stars with internal photometric errors (as given by ALLFRAME) smaller than 0.02 mag are used. Fig. 3 shows that there are no systematic differences between the two runs.

The slope of the straight lines best fitting all the points in both the (V,$\Delta V^{\rm apr}_{\rm dec}$) plane and the (V,$\Delta I^{\rm apr}_{\rm dec}$) plane is $\leq 0.001 \pm 0.002$, and $\leq 0.002 \pm 0.003$ in the (V-I,$\Delta(V-I)^{\rm apr}_{\rm dec}$) plane. The zero point differences are always ≤ 0.01 mag. This ensures the homogeneity of our database, particularly for relative measurements within the CMDs.

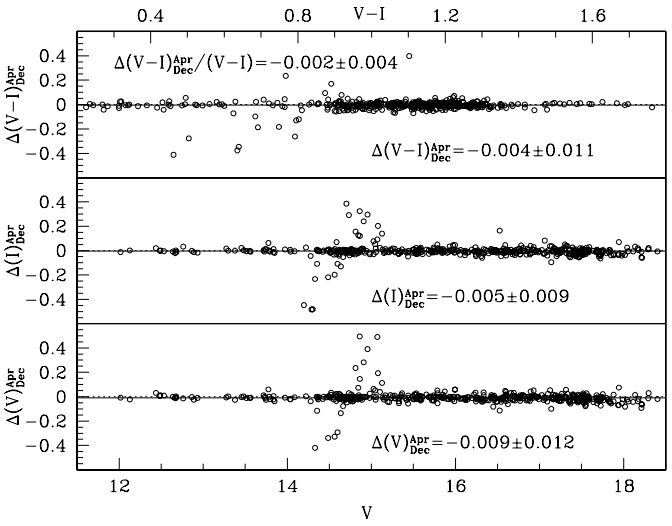

Fig. 3. Comparison of the magnitudes and colors of 456 stars in common between the April and December runs, for the GGC NGC 3201. Stars with photometric internal errors smaller than 0.02 mag have been selected. The mean differences are given in each panel. *Note:* a few NGC 3201 RR Lyrae stars can be identified in the interval $14.2 < V < 15.2$ (lower two panels), and between $0.4 < (V-I) < 0.9$.

5. Parameters for the GGC sample

In order to facilitate the readers work, we present in Tables 3, 4 and 5 the basic parameters available for our GGCs sample[1].

In Table 3 we give the coordinates, the position, and the metallicity of the clusters: right ascension and declination (epoch J2000, columns 3 and 4); Galactic longitude and latitude (columns 5 and 6); Heliocentric (column 7) and Galactocentric (column 8) distances (assuming $R_\odot$=8.0 kpc); spatial components (X,Y,Z) (columns 9, 10 and 11) in the Sun-centered coordinate system (X pointing toward the Galactic center, Y in direction of Galactic rotation, Z toward North Galactic Pole) and, finally, the metallicity given in Rutledge et al. (1997), on both the Zinn & West (1984) and Carretta & Gratton (1997) scales.

In Table 4, the photometric parameters are given. Column 3 lists the foreground reddening; column 4, the V magnitude level of the horizontal branch; column 5, the apparent visual distance modulus; integrated V magnitudes of the clusters are given in column 6; column 7 gives the absolute visual magnitude. Columns 8 to 11 give the integrated color indices (uncorrected for reddening). Column 12 gives the specific frequency of RR Lyrae variables, while column 13 list the horizontal-branch morphological parameter (Lee 1990).

In Table 5, we present the kinematical and structural parameters for the observed clusters. Column 3 gives the heliocentric radial velocity (km/s) with the observational (internal) uncertainty; column 4, the radial velocity relative to the

[1] Unless otherwise stated, the data presented in these tables are taken from the McMaster catalog described by Harris (1996).

Table 3. Identifications, positional data and metallicity estimates for the observed clusters.

ID	Cluster	RA[a] ($^h\ ^m\ ^s$)	DEC[b] ($^\circ\ '\ ''$)	l[c] ($^\circ$)	b[d] ($^\circ$)	$R_\odot$[e] (kpc)	R_{GC}[f] (kpc)	X[g] (kpc)	Y[h] (kpc)	Z[i] (kpc)	[Fe/H] $ZW84$[j]	[Fe/H] $CG97$[k]
1	NGC 104	00 24 05.2	-72 04 51	305.90	-44.89	4.3	7.3	+1.8	-2.5	-3.0	-0.71	-0.78
2	NGC 288	00 52 47.5	-26 35 24	152.28	-89.38	8.1	11.4	-0.1	+0.0	-8.1	-1.40	-1.14
3	NGC 362	01 03 14.3	-70 50 54	301.53	-46.25	8.3	9.2	+3.0	-4.9	-6.0	-1.33	-1.09
4	NGC 1261	03 12 15.3	-55 13 01	270.54	-52.13	16.0	17.9	+0.1	-9.8	-12.6	-1.32	-1.08
5	NGC 1851	05 14 06.3	-40 02 50	244.51	-35.04	12.2	16.8	-4.3	-9.0	-7.0	-1.23	-1.03
6	NGC 1904	05 24 10.6	-24 31 27	227.23	-29.35	12.6	18.5	-7.5	-8.1	-6.2	-1.67	-1.37
7	NGC 2298	06 48 59.2	-36 00 19	245.63	-16.01	10.6	15.6	-4.2	-9.3	-2.9	-1.91	-1.71
8	NGC 2808	09 12 02.6	-64 51 47	282.19	-11.25	9.3	10.9	+1.9	-8.9	-1.8	-1.36	-1.11
9	E3	09 20 59.3	-77 16 57	292.27	-19.02	4.2	7.6	+1.5	-3.7	-1.4	-	-
10	NGC 3201	10 17 36.8	-46 24 40	277.23	+08.64	5.1	8.9	+0.6	-5.0	+0.8	-1.53	-1.24
11	NGC 4372	12 25 45.4	-72 39 33	300.99	-09.88	4.9	6.9	+2.5	-4.2	-0.8	-2.03	-1.88
12	NGC 4590	12 39 28.0	-26 44 34	299.63	+36.05	10.1	10.0	+4.0	-7.1	+5.9	-2.11	-2.00
13	NGC 4833	12 59 35.0	-70 52 29	303.61	-08.01	5.9	6.9	+3.2	-4.8	-0.8	-1.92	-1.71
14	NGC 5139	13 26 45.9	-47 28 37	309.10	+14.97	5.1	6.3	+3.1	-3.8	+1.3	-1.62[1]	-
15	NGC 5897	15 17 24.5	-21 00 37	342.95	+30.29	12.7	7.6	+10.5	-3.2	+6.4	-1.93	-1.73
16	NGC 5927	15 28 00.5	-50 40 22	326.60	+04.86	7.4	4.5	+6.2	-4.1	+0.6	-0.33	-0.64
17	NGC 5986	15 46 03.5	-37 47 10	337.02	+13.27	10.3	4.7	+9.2	-3.9	+2.4	-1.65	-1.35
18	NGC 6093	16 17 02.5	-22 58 30	352.67	+19.46	8.7	3.1	+8.1	-1.0	+2.9	-1.75	-1.47
19	NGC 6121	16 23 35.5	-26 31 31	350.97	+15.97	2.2	6.0	+2.0	-0.3	+0.6	-1.27	-1.05
20	NGC 6101	16 25 48.6	-72 12 06	317.75	-15.82	15.1	11.0	+10.8	-9.8	-4.1	-1.95	-1.76
21	NGC 6171	16 32 31.9	-13 03 13	003.37	+23.01	6.3	3.3	+5.8	+0.3	+2.4	-1.09	-0.95
22	NGC 6266	17 01 12.6	-30 06 44	353.58	+07.32	6.7	1.8	+6.6	-0.7	+0.9	-1.23	-1.02
23	NGC 6304	17 14 32.5	-29 27 44	355.83	+05.38	6.0	2.2	+5.9	-0.4	+0.6	-0.38	-0.66
24	NGC 6352	17 25 29.2	-48 25 22	341.42	-07.17	5.6	3.3	+5.2	-1.8	-0.7	-0.50	-0.70
25	NGC 6362	17 31 54.8	-67 02 53	325.55	-17.57	7.5	5.1	+5.9	-4.0	-2.3	-1.18	-0.99
26	NGC 6397	17 40 41.3	-53 40 25	338.17	-11.96	2.2	6.0	+2.0	-0.8	-0.5	-1.94	-1.76
27	NGC 6496	17 59 02.0	-44 15 54	348.02	-10.01	11.6	4.4	+11.1	-2.4	-2.0	-0.50	-0.70
28	NGC 6544	18 07 20.6	-24 59 51	005.84	-02.20	2.5	5.5	+2.5	+0.3	-0.1	-1.48	-1.20
29	NGC 6541	18 08 02.2	-43 42 20	349.29	-11.18	7.4	2.1	+7.2	-1.4	-1.4	-1.79	-1.53
30	NGC 6624	18 23 40.5	-30 21 40	002.79	-07.91	7.9	1.2	+7.8	+0.4	-1.1	-0.50	-0.70
31	NGC 6626	18 24 32.9	-24 52 12	007.80	-05.58	5.7	2.5	+5.7	+0.8	-0.6	-1.23	-1.03
32	NGC 6638	18 30 56.2	-25 29 47	007.90	-07.15	8.2	1.5	+8.0	+1.1	-1.0	-1.00	-0.90
33	NGC 6637	18 31 23.2	-32 20 53	001.72	-10.27	8.2	1.5	+8.1	+0.2	-1.5	-0.72	-0.78
34	NGC 6656	18 36 24.2	-23 54 12	009.89	-07.55	3.2	5.0	+3.1	+0.5	-0.4	-1.64[1]	-
35	NGC 6681	18 43 12.7	-32 17 31	002.85	-12.51	8.7	2.0	+8.5	+0.4	-1.9	-1.64	-1.35
36	NGC 6717	18 55 06.2	-22 42 03	012.88	-10.90	7.1	2.4	+6.8	+1.6	-1.3	-1.33	-1.09
37	NGC 6723	18 59 33.2	-36 37 54	000.07	-17.30	8.6	2.6	+8.2	+0.0	-2.5	-1.12	-0.96
38	NGC 6752	19 10 51.8	-59 58 55	336.50	-25.63	3.9	5.3	+3.2	-1.4	-1.7	-1.54	-1.24
39	NGC 6809	19 39 59.4	-30 57 44	008.80	-23.27	5.3	3.9	+4.8	+0.7	-2.1	-1.80	-1.54

In the following cases, the [Fe/H] values were taken directly from ([1]) ZW84.

[a] Right Ascension (2000)
[b] Declination (2000)
[c] Galactic Longitude
[d] Galactic Latitude
[e] Heliocentric Distance
[f] Galactocentric Distance

Sun-Centered coordinates:
[g] X: Toward the Galactic Center
[h] Y: in direction of Galactic rotation
[i] Z: Towards North Galactic Plane

[Fe/H] (From Rutledge et al. 1997):
[j] in the ZW84 scale
[k] in the CG97 scale

local standard of rest; column 5, the concentration parameter ($c = \log(r_t/r_c)$); a 'c' denotes a core-collapsed cluster; columns 6 and 7, the core and the half mass radii in arcmin; column 8, the logarithm of the core relaxation time, in years; and column 9 the logarithm of the relaxation time at the half mass radius. Column 10, the central surface brightness in V; and column 11, the logarithm of central luminosity density (Solar luminosities per cubic parsec).

Table 4. Photometric Parameters.

ID	Cluster	$E(B-V)^a$	V_{HB}^b	$(m-M)_V^c$	$V_t{}^d$	$Mv_t{}^e$	$U-B^f$	$B-V^f$	$V-R^f$	$V-I^f$	S_{RR}^g	HBR^h
1	NGC 104	0.05	14.05*	13.32	3.95	-9.37	0.37	0.88	0.53	1.14	0.4	-0.99
2	NGC 288	0.03	15.40*	14.64	8.09	-6.55	0.08	0.65	0.45	0.94	4.8	0.98
3	NGC 362	0.05	15.43	14.75	6.40	-8.35	0.16	0.77	0.49	1.01	5.9	-0.87
4	NGC 1261	0.01	16.68*	16.05	8.29	-7.76	0.13	0.72	0.45	0.93	14.9	-0.71
5	NGC 1851	0.02	16.18*	15.49	7.14	-8.35	0.17	0.76	0.49	1.01	10.1	-0.36
6	NGC 1904	0.01	16.15*	15.53	7.73	-7.80	0.06	0.65	0.44	0.91	5.3	0.89
7	NGC 2298	0.13	16.11	15.54	9.29	-6.25	0.17	0.75	0.54	1.11	9.5	0.93
8	NGC 2808	0.23	16.30*	15.55	6.20	-9.35	0.28	0.92	0.57	1.18	0.4	-0.49
9	E 3	0.30	14.80	14.07	11.35	-2.72	-	-	-	-	0.0	-
10	NGC 3201	0.21	14.75*	14.17	6.75	-7.42	0.38	0.96	0.62	1.23	91.3	0.08
11	NGC 4372	0.42	15.30	14.76	7.24	-7.52	0.31	1.10	0.72	1.50	0.0	1.00
12	NGC 4590	0.04	15.75*	15.14	7.84	-7.30	0.04	0.63	0.46	0.94	49.3	0.17
13	NGC 4833	0.33	15.45	14.87	6.91	-7.96	0.29	0.93	0.63	1.33	11.8	0.93
14	NGC 5139	0.12	14.53	13.92	3.68	-10.24	0.19	0.78	0.51	1.05	12.2	-
15	NGC 5897	0.08	16.35	15.77	8.53	-7.24	0.08	0.74	0.50	1.04	8.9	0.86
16	NGC 5927	0.47	16.60	15.81	8.01	-7.80	0.85	1.31	0.79	1.63	0.0	-1.00
17	NGC 5986	0.27	16.50	15.90	7.52	-8.38	0.30	0.90	0.58	1.22	4.4	0.97
18	NGC 6093	0.18	16.25*	15.25	7.33	-7.92	0.21	0.84	0.56	1.11	4.1	0.93
19	NGC 6121	0.36	13.36*	12.78	5.63	-7.15	0.43	1.03	0.69	1.42	70.4	-0.06
20	NGC 6101	0.04	16.60	16.02	9.16	-6.86	0.06	0.68	0.50	-	19.8	0.84
21	NGC 6171	0.33	15.65*	15.01	7.93	-7.08	0.69	1.10	0.72	1.45	32.5	-0.73
22	NGC 6266	0.47	16.25	15.59	6.45	-9.14	0.52	1.19	0.74	1.58	19.1	0.32
23	NGC 6304	0.52	16.25	15.49	8.22	-7.27	0.82	1.31	0.77	1.70	0.0	-1.00
24	NGC 6352	0.21	15.25*	14.39	7.96	-6.43	0.64	1.06	0.66	1.50	0.0	-1.00
25	NGC 6362	0.09	15.35*	14.65	7.73	-6.92	0.29	0.85	0.56	1.14	56.4	-0.58
26	NGC 6397	0.18	12.95*	12.31	5.73	-6.58	0.12	0.73	0.49	1.03	0.0	0.98
27	NGC 6496	0.13	16.47	15.72	8.54	-7.18	0.45	0.98	-	-	0.0	-1.00
28	NGC 6544	0.74	14.90	14.28	7.77	-6.51	0.73	1.46	0.98	1.92	-	1.00
29	NGC 6541	0.12	15.30	14.72	6.30	-8.42	0.13	0.76	0.49	1.01	0.0	1.00
30	NGC 6624	0.27	16.11	15.32	7.87	-7.45	0.60	1.11	0.67	1.42	1.0	-1.00
31	NGC 6626	0.41	15.70	15.07	6.79	-8.28	0.46	1.08	0.69	1.41	6.4	0.90
32	NGC 6638	0.40	16.50	15.80	9.02	-6.78	0.56	1.15	0.72	1.50	38.9	-0.30
33	NGC 6637	0.17	15.85	15.11	7.64	-7.47	0.48	1.01	0.62	1.28	0.0	-1.00
34	NGC 6656	0.34	14.25*	13.55	5.10	-8.45	0.28	0.98	0.68	1.42	7.5	0.91
35	NGC 6681	0.07	15.70*	14.93	7.87	-7.06	0.12	0.72	0.47	0.99	3.0	0.96
36	NGC 6717	0.21	15.56	14.90	9.28	-5.62	0.35	1.00	0.65	1.37	5.6	0.98
37	NGC 6723	0.05	15.45*	14.82	7.01	-7.81	0.21	0.75	0.50	1.05	21.8	-0.08
38	NGC 6752	0.04	13.80*	13.08	5.40	-7.68	0.07	0.66	0.43	0.93	0.0	1.00
39	NGC 6809	0.07	14.45*	13.82	6.32	-7.50	0.11	0.72	0.48	1.00	10.0	0.87

The HB levels (column 4) with an asterisk have been measured directly on our CMDs.

[a] Foreground reddening
[b] HB Level
[c] Apparent visual distance modulus
[d] Integrated V mag. of clusters
[e] Absolute visual magnitude
[f] Integrated color indices
[g] Specific frequency of RR Lyrae variables
[h] HB ratio: $HBR = (B-R)/(B+V+R)$

6. The Color-Magnitude Diagrams

In this section the V vs. $(V-I)$ CMDs for the 39 GGCs and the covered fields are presented.

The same color and magnitude scale has been used in plotting the CMDs, so that differential measures can be done directly using the plots. Two dot sizes have been used, with the bigger ones corresponding to the better measured stars, normally selected on the basis of error (≤ 0.1) and sharpness parameter (Stetson 1987). In some exceptional cases, a selection on radius is also done in order to make evident the cluster stars over the field stars, or to show differential reddening effects. The smaller size dots show all the measured stars with errors (as calculated by DAOPHOT) smaller than 0.15 mag.

The images of the fields are oriented with the North at the top and East on the left side. As explained in Sect. 2, each field

Table 5. Kinematics, and Structural Parameters

ID	Cluster	$V_{\rm r}^{\rm a}$	$V_{\rm LSR}^{\rm b}$	$c^{\rm c}$	$r_{\rm c}^{\rm d}$	$r_{\rm h}^{\rm e}$	$lg(t_{\rm c})^{\rm f}$	$lg(t_{\rm h})^{\rm g}$	$\mu_{\rm V}^{\rm h}$	$\rho_0^{\rm i}$
01	NGC 104	-18.7 ± 0.2	-28.0	2.04	0.37	2.79	7.99	9.24	14.43	4.87
02	NGC 288	-46.6 ± 0.4	-53.9	0.96	1.42	2.22	9.09	8.99	19.95	1.84
03	NGC 362	$+223.5 \pm 0.5$	$+213.3$	1.94c	0.17	0.81	7.79	8.43	14.88	4.74
04	NGC 1261	$+68.2 \pm 4.6$	$+53.4$	1.27	0.39	0.75	8.79	8.81	17.65	2.97
05	NGC 1851	$+320.9 \pm 1.0$	$+302.1$	2.24	0.08	0.52	7.41	8.50	14.15	5.17
06	NGC 1904	$+207.5 \pm 0.5$	$+188.3$	1.72	0.16	0.80	7.87	8.66	16.23	4.01
07	NGC 2298	$+148.9 \pm 1.2$	$+129.8$	1.28	0.34	0.78	8.02	8.36	18.79	2.90
08	NGC 2808	$+93.6 \pm 2.4$	$+80.1$	1.77	0.26	0.76	8.35	8.77	15.17	4.62
09	E3	-	-	-	0.75	1.87	2.06	-	23.10	1.12
10	NGC 3201	$+494.0 \pm 0.2$	$+481.9$	1.31	1.45	2.68	8.82	8.79	18.77	2.69
11	NGC 4372	$+72.3 \pm 1.3$	$+63.8$	1.30	1.75	3.90	8.88	9.23	20.51	2.19
12	NGC 4590	-95.2 ± 0.4	-97.1	1.64	0.69	1.55	8.60	8.90	18.67	2.53
13	NGC 4833	$+200.2 \pm 1.2$	$+192.7$	1.25	1.00	2.41	8.79	8.77	18.45	3.07
14	NGC 5139	$+232.3 \pm 0.5$	$+229.4$	1.24	2.58	4.18	9.76	9.72	16.77	3.13
15	NGC 5897	$+101.5 \pm 1.0$	$+110.0$	0.79	1.96	2.11	9.78	9.31	20.49	1.38
16	NGC 5927	-115.7 ± 3.1	-114.5	1.60	0.42	1.15	8.53	8.71	17.45	3.90
17	NGC 5986	$+88.9 \pm 3.7$	$+94.3$	1.22	0.63	1.05	8.97	8.78	17.56	3.31
18	NGC 6093	$+9.3 \pm 3.1$	$+19.7$	1.95	0.15	0.65	7.60	8.32	15.19	4.82
19	NGC 6121	$+70.2 \pm 0.3$	$+79.8$	1.59	0.83	3.65	7.57	8.64	17.88	3.83
20	NGC 6101	$+361.4 \pm 1.7$	$+357.2$	0.80	1.15	1.71	9.44	9.22	20.12	1.63
21	NGC 6171	-33.8 ± 0.3	-20.6	1.51	0.54	2.70	8.10	8.75	18.84	3.14
22	NGC 6266	-65.8 ± 2.5	-56.3	1.70c	0.18	1.23	7.54	8.55	15.35	5.15
23	NGC 6304	-107.3 ± 3.6	-97.4	1.80	0.21	1.41	7.45	8.56	17.34	4.40
24	NGC 6352	-120.9 ± 3.0	-116.7	1.10	0.83	2.00	8.64	8.71	18.42	3.05
25	NGC 6362	-13.1 ± 0.6	-15.1	1.10	1.32	2.18	9.09	8.83	19.19	2.27
26	NGC 6397	$+18.9 \pm 0.1$	$+21.4$	2.50c	0.05	2.33	4.93	8.35	15.65	5.69
27	NGC 6496	-112.7 ± 5.7	-107.0	0.70	1.05	1.87	8.46	8.46	20.10	1.94
28	NGC 6544	-27.3 ± 3.9	-15.7	1.63c	0.05	1.77	5.23	7.82	17.13	5.78
29	NGC 6541	-156.2 ± 2.7	-150.3	2.00c	0.30	1.19	8.04	8.58	15.58	4.36
30	NGC 6624	$+53.9 \pm 0.6$	$+63.9$	2.50c	0.06	0.82	6.71	8.50	15.42	5.24
31	NGC 6626	$+17.0 \pm 1.0$	$+28.5$	1.67	0.24	1.56	7.73	8.78	16.08	4.73
32	NGC 6638	$+18.1 \pm 3.9$	$+29.4$	1.40	0.26	0.66	8.00	8.02	17.27	4.06
33	NGC 6637	$+39.9 \pm 2.8$	$+49.3$	1.39	0.34	0.83	8.40	8.69	16.83	3.83
34	NGC 6656	-148.9 ± 0.4	-137.2	1.31	1.42	3.26	8.62	8.86	17.32	3.65
35	NGC 6681	$+218.6 \pm 1.2$	$+227.9$	2.50c	0.03	0.93	5.82	8.40	15.28	5.42
36	NGC 6717	$+22.8 \pm 3.4$	$+34.6$	2.07c	0.08	0.68	6.61	8.14	16.48	4.68
37	NGC 6723	-94.5 ± 3.6	-86.7	1.05	0.94	1.61	9.02	8.94	17.92	2.82
38	NGC 6752	-24.5 ± 1.9	-24.4	2.50c	0.17	2.34	6.95	8.65	15.20	4.92
39	NGC 6809	$+174.8 \pm 0.4$	$+183.4$	0.76	2.83	2.89	9.40	8.89	19.13	2.15

[a]Heliocentric radial velocity
[b]Radial velocity relative to the(LSR)
[c]Concentration parameter $[c = log(r_{\rm t}/r_{\rm c})]$
[d]The core radii
[e]The core median radii
[f]Log. of relaxation time in years
[g]Log. of core relaxation time at $r_{\rm h}$
[h]Central surface brightness
[i]Log. of central luminosity density

covers $3.77 \times 3.77(')^2$, and the overlaps between fields of the same object are about $20 - 25\%$ of the area. For some clusters, only short exposures were obtained for the central fields.

In the next subsections, we present the single CMDs and clusters, and give some references to the best existing CMDs. This is by no means a complete bibliographical catalog: a large number of CMDs are available in the literature for many of the clusters of this survey, but we will concentrate just on the best CCD photometric works. The tables with the position and photometry of the measured stars will be available via a web interface at IAC and Padova in the near future.

NGC 104 (47 Tucanae). (Fig. 4)

The cluster 47 Tucanae is (after ω Centauri) the second brightest globular cluster in the sky, and consequently a lot of work has been done on this object. 47 Tucanae has been often indicated as the prototype of the metal-rich GGCs, characterized by a well populated red HB (RHB) clump and an extended

RGB that also in our CMD spans ∼2 mag in color from the RHB to the reddest stars at the tip.

A classical CMD of 47 Tucanae is that presented by Hesser et al. (1987) where a composite CMD was obtained from the superposition of B and V CCD photometry for the main sequence (MS) and photographic data for the evolved part of the diagram. The same year, Alcaino & Liller (1987a) published a BVI CCD photometry. One year later, Armandroff (1988) presented the RGB V and I bands photometry for this cluster (together with other five). In 1994, Sarajedini & Norris (1994) presented a study of the RGB and HB stars in the B and I bands. Sosin et al. (1997a) and Rich et al. (1997) have published a B,V photometry based on HST data.

A recent work in the V and I bands has been presented by Kaluzny et al. (1998), who focussed their study on the variable stars. They do not find any RR-Lyrae, but many other variables (mostly located in the BSS region), identified as binary stars. As already stated by these authors, a small difference is found between their and our photometry. Indeed, their magnitudes coincide with ours at ~ 12.5 mag in both bands, but there is a small deviation from linearity of ~ -0.015 magnitudes per magnitude (with the Kaluzny et al. stars brighter than ours), in both bands (computed from 90 common stars with small photometric errors) within a magnitude range of ~ 3 mag. We are confident that our calibration, within the quoted errors, is correct, as further confirmed by the comparison with other authors for other objects, as discussed below. Although small, these differences could be important in relative measures, if they appear randomly in different CMDs. For example, in this case, the $\Delta V_{\rm TO}^{\rm HB}$ parameter is ~ 0.05 mag smaller in Kaluzny et al. (1998) CMD than in our one, implying, for the 47 Tuc metallicity, an age difference of ~ 0.8 Gyrs. We want to stress the importance of a homogeneous database for a reliable measurement of differential parameters on the CMDs.

NGC 288 and NGC 362. (Figs. 5 and 6)

The diagram of NGC 288 is well defined and presents an extended blue horizontal branch (EBHB) which extends from the blue side of the RR-Lyrae region, to just above the TO. Conversely, NGC 362 has a populated RHB with just a few blue HB stars.

These two clusters define one of the most studied second parameter couple: despite their similar metallicities, their HB morphologies are different. Much work have been done on both clusters in order to try to understand the origin of such differences: Bolte (1989) and Sarajedini & Demarque (1990) in the B and V bands, and Green & Norris (1990) in the B and R bands, based on homogeneous CCD photometry, obtain an age difference of ~ 3 Gyrs, NGC 288 being older than NGC 362. A similar conclusion is obtained in our study (Paper III), where NGC 362 is found $\sim 20\%$ younger than NGC 288. It has also been proposed (e.g. Green & Norris 1990) that these age differences might be responsible of the HB differences between the two clusters. On the other side, Buonanno et al. (1998) and Salaris & Weiss (1998) do not find significant age differences. Another B,V photometry of NGC 362 based on HST data is in Sosin et al. (1997a).

It might be worth to remark here that, as it will be discussed in Paper II, there are clusters with different HB morphologies, though with the same metallicities and ages (within errors). This means that the analysis of a single couple of GGCs can not be considered conclusive for understanding the second parameter problem, while a large scale study (as that feasible with this catalog) can be of more help.

NGC 1261. (Fig. 7)

This cluster is the object with the largest distance in our southern hemisphere sample. It is located at ~ 16 kpc from the Sun.

Three major CCD CMDs have been published for NGC 1261: Bolte & Marleau (1989) in B, V, Alcaino et al. (1992) in B, V, R, I, and Ferraro et al. (1993b) in the B and V bands.

The CMD is characterized by an HB which is similar to the HB of NGC 1851. From here on, clusters with an HB well populated both on the red and blue side of the RR-Lyrae gap will be named bimodal HB clusters, though a more objective classification would require taking into account the color distribution of stars along the HB including the RR Lyrae (Catelan et al. 1998). NGC 1261 has a metallicity very close to that of the previous couple; Chaboyer et al. (1996), Richer et al. (1996) and Rosenberg et al. (Paper III) find that it is younger (similar in age to NGC 362) than the bulk of GGCs. A blue straggler (BS) is clearly visible in Fig. 7.

NGC 1851. (Fig. 8)

This cluster has a bimodal HB, with very well defined RHB and blue HB (BHB). Also in this case, a BS sequence is visible in Fig. 8. It is curious that, again, a bimodal cluster results to be younger than the GGCs bulk. From the 34 clusters in the present catalog, only 4 result to be surely younger, i.e. the already described NGC 362 and NGC 1261, this cluster, and NGC 2808: three of them have a bimodal HB (cf. Rosenberg et al. 1999 for a detailed discussion). There exist other two recent (V, I) CCD photometries of NGC 1851 by Walker (1998) and Saviane et al. (1998). The three photometries are all in agreement within the errors, confirming our calibration to the standard system. A CMD of NGC 1851 in the B,V bands from HST is in Sosin et al. (1997a). Older CCD photometries are found in Alcaino et al (1990a) (B, V, I bands) and Walker (1992) (B, V bands)

NGC 1904 (M 79). (Fig. 9)

M 79 is the farthest cluster ($R_{\rm GC} = 18.5$ kpc) from the Galactic center in our sample. The main feature in the CMD of Fig. 9 is the EBHB. Previous CMDs from CCD photometry are in Heasley et al. (1983) (U, B, V bands), Gratton & Ortolani (1986) (B, V bands), Ferraro et al. (1993a) (B, V bands), Alcaino et al. (1994) (B, V, R, I bands), and Kravtsov et al.

(1997) (U, B, V bands), and the B,V photometry from HST in Sosin et al. (1997a).

NGC 2298. (Fig. 10)

This cluster is poorly sampled, particularly for the bright part of the diagram (due to problems with a short exposure). Only four BHB stars are present in the HB region. Recent photometric works on this object are in Gratton & Ortolani (1986) (B, V bands), Alcaino & Liller (1986a) (B, V, R, I bands), Janes & Heasley (1988) (U, B, V bands), and Alcaino et al. (1990b) (B, V, R, I bands).

NGC 2808. (Fig. 11)

This cluster has some differential reddening (Walker 1999), as it can be inferred also from the broadening of the sequences in the CMD of Fig. 11, and a moderate field contamination. The most interesting features of the CMD are the bimodal HB and the EBHB tail with other two gaps, as extensively discussed in Sosin et al. (1997b). As previously discussed, NGC 2808 is another bimodal HB cluster at intermediate metallicity with a younger age (Rosenberg et al. 1999). Apart from the already quoted B, and V band photometry from HST data by Sosin et al. (1997b), there are many other CCD photometries: Gratton & Ortolani (1986) (B, V bands), Buonanno et al. (1989) (B, V bands), Ferraro et al. (1990) (B, V bands), Alcaino et al. (1990c) (B, V, R, I bands), Byun & Lee (1993), Ferraro et al. (1997) (V, I bands), and more recently Walker (1999) (B, V bands).

E3. (Fig. 12)

This cluster is one of the less populated clusters in our Galaxy, resembling some Palomar-like globular as Pal 1 (Rosenberg et al. 1998). As in Pal 1, there are no HB stars in the CMD, and the entire population of observed stars is smaller than 1000 objects. E3 is suspected to have a metallicity close to that of Pal 1. From the $\delta(V-I)_{@2.5}$ (Paper III) measured on Fig. 12, E3 is coeval with the other GGCs of similar metallicity, though the result is necessarily very uncertain, due to the high contamination and the small number of RGB stars. E3 is the cluster with the better defined MS binary sequence (Veronesi et al. 1996), which can be also seen in Fig. 12. Previous CCD CMDs are in McClure et al. (1985) (B, V bands), Gratton & Ortolani (1987) (B, V bands), and Veronesi et al. (1996) (B, V, R, I bands).

NGC 3201. (Fig. 13)

The two lateral fields presented in Fig. 13 were observed in both runs, in order to test the homogeneity of the data and instrumentation (see Sect. 4). The HB of NGC 3201 has a bimodal appearance, though it is not younger than the bulk of GGCs of the same metallicity group, at variance with the previously discussed cases. It has a small differential reddening. A blue straggler (BS) sequence is visible in Fig. 13. Previous CCD studies of this cluster include Penny (1984) (B, V, I bands), Alcaino et al. (1989) (B, V, R, I bands), Brewer et al. (1993) (U, B, V, I bands) and Covino & Ortolani (1997) (B, V bands).

NGC 4372. (Fig. 14)

The principal characteristic of the CMD of this cluster is the broadening of all the sequences, consequence of the high differential reddening, probably due to the Coal-sack Nebulae. In the CMD of Fig. 14 the darker dots are from the stars in the lowest reddening region (south east) of the observed fields. We have computed the reddening field for this cluster from the shift of the CMDs obtained in different positions, finding that it is homogeneously distributed in space and quite easy to correct by a second order polynomial surface. Two previous CCD photometries can be found in Alcaino et al. (1991) (B, V, R, I bands) and Brocato et al. (1996) (B, V bands).

NGC 4590 (M 68). (Fig. 15)

This cluster is probably the lowest metallicity cluster of the present sample. It has a well defined CMD, with an HB populated on both sides of the instability strip, and including some RR-Lyrae stars. It has sometimes been classified as one of the oldest GGCs (Salaris et al 1997), and, in fact, we find that M68 is old, though coeval with the rest of the metal poor clusters (Paper III). Other CCD CMDs for this cluster are in McClure et al. (1987) (B, V bands), Alcaino et al. (1990d) (B, V, R, I bands) and Walker (1994) (B, V, I bands).

NGC 4833. (Fig. 16)

NGC 4833 is another metal-poor cluster, with an extended BHB, likely with gaps, for which we have not found any previous CCD photometry.

NGC 5139 (ω Centauri). (Fig. 17)

NGC 5139 is the intrinsically brightest cluster in our Galaxy. Apart from this, there are many other properties of ω Centauri which make it a very particular object. Its stellar population shows metallicity variations as large as ~ 1.5 dex from star to star (Norris et al. 1996). Its overall properties suggest that this clusters could have a different origin from the bulk of GGCs. It has an extended BHB and probably numerous BSS. The broad sequences in the CMD are mainly due to the metallicity variations though likely there is some differential reddening in the field of ω Centauri. Due to its peculiarities, ω Centauri has been (and is!) extensively studied; there is a large number of photometries, and we cannot cite all of them. The most recent and interesting CCD CMDs are in: Alcaino & Liller (1987b), who present a multi-band (B, V, R, I) photometry, but poorly sampled, specially for the evolved part of the diagram; Noble et al. (1991) present a deep B, V diagram, where the MS is well sampled, but the RGB is not so clear and only 3-5 stars are present in the HB; Elson et al. (1995) present a HST V, I photometry of the MS; Lynga (1996) presents a $BVRI$ study of the evolved part of the diagram (~ 2 mag be-

low the HB); Kaluzny et al. (1996, 1997) present a V, I CMD covering more than 10^5 stars.

NGC 5897. (Fig. 18)

NGC 5897 is a metal poor cluster with a blue, not extended HB, typical for its metallicity. All the sequences of Fig. 18 are well defined and populated, including a BS sequence. Two CCD photometric studies exist for this cluster: Sarajedini (1992) (B, V bands) and Ferraro et al. (1992) (U, B, V, I bands).

NGC 5927. (Fig. 19)

NGC 5927 has the highest metallicity among the objects of our catalog. It has, as most of the GGCs with [Fe/H]> -0.8, a well populated red horizontal branch (RHB), and an extended RGB, which, in our CMD, covers more than $\sim$2.5 mag in $(V - I)$, from the RHB (partially overlapped with the RGB) to the reddest stars of the RGB tip. It has a high reddening, possibly differential, judging from the broadening of the RGB, and, due to its location (projected towards the Galactic center), the field object contamination (disk and bulge stars) is very high. Previous CCD photometries are in Friel & Geisler (1991) (Washington photometry), Sarajedini & Norris (1994) (B, V bands), Samus et al. (1996) (B, V, I bands), Sosin et al. (1997a), and Rich et al. (1997) (HST B, V bands).

NGC 5986. (Fig. 20)

To our knowledge, this is the first CCD photometry for this cluster. NGC 5986 is an intermediate metallicity cluster, but with a metal-poor like HB. The broadening of the CMD suggests some differential reddening. Contamination by field stars is clearly visible, as expected on the basis of the position within the Galaxy of this cluster.

NGC 6093 (M 80). (Fig. 21)

NGC 6093 is a bright and moderately metal poor cluster, and one of the densest globular clusters in the Galaxy. It has an EBHB, which extends well below the TO as clearly visible also in the CMD of Fig. 21, with gaps (Ferraro et al. 1998). Three recent CCD photometries that cover the entire object, with CMD from the brightest stars to above the TO exist for this cluster: Brocato et al. (1998) (B, V bands) and Ferraro et al. (1998) (HST U, V, and far-UV (F160BW) bands). A ground-based multicolor U, B, V, I CCD CMD has been published also by Alcaino et al. (1998).

NGC 6101. (Fig. 22)

NGC 6101 was observed under not very good seeing conditions, and this is the reason for the brighter limiting magnitude. Its CMD has the morphology expected for a metal-poor cluster: the HB is predominantly blue, and the giant branch is steep. In Fig. 22 we note that, starting from the BSS sequence, there is a sequence of stars parallel to the RGB on its blue side. In view of the position of the cluster (l, b)=(318,-16) these can unlikely be bulge stars; it is possible that on the same line of sight there is an open cluster, though the slope of the two RGBs are quite similar, implying an unlikely similar metallicity. A larger field coverage of NGC 6101 is desirable. The only previous CCD photometry that exists for this cluster is the B and V study by Sarajedini & Da Costa (1991), which shows these stars in the same CMD location. However, being the background-foreground stellar contamination heavier, the sequences we discussed can hardly be seen.

NGC 6121 (M 4). (Fig. 23)

This cluster is the closest GGC, located approximately at $\sim$ 2.2 kpc from the Sun, though, due to the large reddening caused by the nebulosity in Scorpio-Ophiuchus, it has an apparent visual distance modulus larger than NGC 6397. The reddening is differential, though (as in the case of NGC 4372) it is homogeneously distributed in space. The mean regions of the CMD can be improved using an appropriate second order polynomial fit to the reddening distribution, at least on the two fields shown in Fig. 23. The stars from the southern field have been plotted as darker dots; they are located on the redder (more reddened) part of the CMD. The two most recent CMD of M4 are in Ibata et al. (1999) (V, I, U filters) and Pulone et al. (1999), who present (near IR) HST studies of the faint part of the MS and of the WD sequence. Other recent CMDs from the RGB tip to below the MSTO are in Alcaino et al. (1997a), who presented an $UBVI$ CCD photometry, and Kanatas et al. (1995), who obtained a composite (B, V) CMD from $V \sim 12$ to $V \sim 25$.

NGC 6171 (M 107). (Fig. 24)

Previous CCD studies of NGC 6171 are the (J, K) and (B, V) photometry by Ferraro et al. (1995 and 1991, respectively). This cluster is affected by a moderate reddening, which could be slightly differential. It has a RHB, with a few stars bluer than the instability strip blue edge.

NGC 6266 (M 62). (Fig. 25)

This cluster is located very close to the Galactic center, and it has a high differential reddening. It seems to have both a RHB and a BHB resembling the HB of NGC 1851. Previous B, V bands CCD works are in Caloi et al. (1987), and Brocato et al. (1996). A de-reddened CMD and RR-Lyrae stars are also studied in Malakhova et al. (1997).

NGC 6304. (Fig. 26)

NGC 6304 is a high metallicity cluster very close to the Galactic center, and has one of the highest reddenings in our sample. It has some disk and bulge star contamination. There is a second RGB fainter and redder than the main RGB (bulge star contamination or a more absorbing patch?), but the most noticeable feature is the extremely long RGB. The reddest star of its RGB is located $\sim$3.7 mag redward from the RHB! To our knowledge, this is the most extended RGB known for a GGC.

The most recent CCD CMD for this cluster comes from the V and K photometry by Davidge et al. (1992) which covers the hottest RGB stars and the HB.

NGC 6352. (Fig. 27)

NGC 6352 is another high metallicity bulge GGC, with a CMD typical of a cluster with this metal content. The most recent CCD study on this cluster is in Fullton et al. (1995), where a $VI_{\rm c}$ CMD from HST data combined with ground-based observations is presented. Another study of the RGB and HB regions of this cluster is presented by Sarajedini & Norris (1994) in the B, V bands.

NGC 6362. (Fig. 28)

NGC 6362 presents a well defined CMD with a bimodal HB. The most recent CMD on this cluster is given by Piotto et al. (1999), who present observations of the center of the cluster obtained with the HST/WFPC2 camera in the B and V bands. The only previous ground-based CCD photometry is in Alcaino & Liller (1986b). Our field has been also observed in the same filters by Walker (priv. comm.), who made available to us his data for a cross-check of the photometric calibration. We find that the two photometries agree within the errors. In particular, we found a zero point difference of 0.02 mag for the V band and 0.01 mag for the I band, with a negligible -0.001 color term difference between Walker and our data. These discrepancies are well within the uncertainties, and allow to further confirm our calibration to the standard (Landolt 1992) system.

NGC 6397. (Fig. 29)

This cluster is the GGC with the smallest apparent distance modulus. Cool et al. (1996) and King et al. (1998) present an extremely well defined CMD of the main sequence of this cluster, from HST data, from just below the TO down to $I = 24.5$, which correspond to a mass of less than $0.1 M_{\odot}$. Other HST studies on this cluster have been presented by Burgarella et al. (1994), De Marchi & Paresce (1994), Cool et al. (1995) and King et al. (1995). Many ground-based CCD data have also been published: Auriere et al. (1990), Anthony-Twarog et al. (1992) (Stromgren photometry), Lauzeral et al. (1992, 1993), Kaluzny (1997) (B, V bands) and Alcaino et al. (1987: B, V bands; 1997b: U, B, V, I bands).

NGC 6496. (Fig. 30)

NGC 6496 is another metal rich GGC which presents an extended RGB. In this case, the reddest stars are ~ 2 mag redder than the RHB. It has also a remarkably tilted RHB, already noted by Richtler et al. (1994), who present a CCD (B, V) photometry of this cluster; Armandroff (1988) gives (V, I) CCD photometry. A tilted RHB can be noted not only in this CMD, but also in the CMDs of most of the very metal-rich clusters of our sample. Such a feature is usually not present in the canonical models. The RHB is well populated, and there are two stars located on the BHB region. This is quite unusual considering the metallicity of NGC 6496, and it would be interesting to study the membership and to obtain a CMD on a larger field. Another CCD photometry of this cluster is in Friel & Geisler (1991) in the Washington system. Sarajedini & Norris (1994) present a B and V photometry for the RGB and HB region.

NGC 6541. (Fig. 31)

NGC 6541 is located rather close to the Galactic center, and this explains the high field star contamination of the CMD. It has a BHB, as expected from its metal content. The only previous CCD study of this cluster is the multicolor photometry by Alcaino et al. (1997c).

NGC 6544. (Fig. 32)

This is an example of a terrible "spotty" field with a high (the highest in our sample) and highly differential reddening, due to the location of NGC 6544, which is very close to the Galactic plane and projected towards the Galactic center. Interestingly enough, despite its intermediate metallicity, there are only BHB stars. Probably, the use of the HST in this case is almost inevitable if we want to estimate the age of this kind of clusters. We have not found any previous CCD photometry of this cluster.

NGC 6624. (Fig. 33)

Another member of the metal-rich group is presented in Fig. 33. Despite of being the cluster closest to the Galactic center, NGC 6624 has a moderate field star contamination, and a very well defined RGB and RHB. The reddest stars of the RGB are in this case ~ 2.2 mag redder than the RHB.

Richtler et al. (1994) present a B and V CCD CMD of this cluster extending well below the TO, while Sarajedini & Norris (1994) present a photometric study of the RGB and HB in the same bands. A B, V CMD from HST data is in Sosin & King (1995) and Sosin et al. (1997a).

NGC 6626 (M 28). (Fig. 34)

Again a high differential reddening is present in the field of NGC 6626, which is located close to the Galactic center. NGC 6626 seems to have an extended BHB, and maybe a few RHB stars, though the field star contamination makes it rather difficult to see them. Previous CCD photometry is given by Davidge et al. (1996), who present a deep near infrared photometry.

NGC 6637 (M 69). (Fig. 35)

The CMD of NGC 6637 presents the typical distribution in color for the RGB stars discussed for other metal rich clusters, with the reddest stars ~ 2.4 mag redder than the RHB. Previous B and V CCD photometry is presented by Richtler et al. (1994), and the RGB-HB region is also studied by Sarajedini & Norris (1994) in the same bands.

NGC 6638. Fig. 36

Affected by high differential reddening, the CMD this cluster is not very well defined. However, the HB is clearly populated on both sides of the instability strip, and probably there are many RR-Lyrae. We have not found any previous CCD photometries of this cluster.

NGC 6656 (M 22). (Fig. 37)

A possible internal dispersion in metallicity has been proposed for M22. It presents an EBHB with some HB stars as faint as the TO, and several possible RR-Lyrae stars. It is close to the Galactic center and to the Galactic plane, with a high reddening.

Piotto & Zoccali (1999) published the most recent study of this cluster. From a combination of HST data and ground based CCD photometry, they produced a CMD extending from the tip of the RGB to below $0.2M_{\odot}$. Anthony-Twarog et al. (1995) present $uvbyCa$ data for over 300 giant and HB stars, while in Davidge & Harris (1996) there is a deep near infrared study.

NGC 6681 (M 70). (Fig. 38)

NGC 6681 has a predominantly blue HB with a few HB stars on the red side of the instability strip. Brocato et al. (1996) present the only other available CCD photometry for this cluster in the B and V bands.

NGC 6717 (Palomar 9). (Fig. 39)

NGC 6717 is a poorly populated cluster (as most of the "Palomar-like" objects), and the CMD is contaminated by bulge stars. The RGB is difficult to identify, and its HB is blue, resembling that of NGC 288. Notice that there is a very bright field star close to the cluster, located at the north side of it. Brocato et al. (1996) present the first CCD photometry for this cluster; their B and V CMD resembles that of Fig. 39. Recently, Ortolani et al. (1999) presented a new CMD, in the same bands, but the CMD branches are more poorly defined.

NGC 6723. (Fig. 40)

NGC 6723 has both a red and blue HB, and the overall morphology is typical of a cluster of intermediate metallicity. Alcaino et al. (1999) present the most recent CCD study (multicolor photometry), with a CMD extending down to $V \sim 21$. Fullton & Carney (1996) have obtained a deep B and V photometry, extending to $V \sim 24$, though the results of this study have not been completely published, yet.

NGC 6752. (Fig. 41)

NGC 6752 has been largely studied in the past. It has a very well defined EBHB. Penny & Dickens (1986) presented a B and V CCD study from a combination of data from two telescopes, and published a CMD from the RGB tip to $V \sim 24$ mag, though with a small number of measured stars. In the same year, Buonanno et al. (1986) present a CMD in the same bands for stars from ~ 1 mag above the TO to ~ 5 mag below it. More recently, Renzini et al. (1996) and Rubenstein & Baylin (1997) published a CMD from HST data.

NGC 6809 (M 55). (Fig. 42)

Also the CMD of NGC 6809 is typical for its (low) metallicity. A very well defined BS sequence is visible in Fig. 42. The most recent CCD study is in Piotto & Zoccali (1999), who study the cluster luminosity function based on deep HST data combined with ground-based CCD data for the evolved part of the CMD. Zaggia et al. (1997) present V and I CCD photometry of ~ 34000 stars covering an entire quadrant of the cluster (out to ~ 1.5 times the tidal radius) down to $V \sim 21$. Mateo et al. (1996) and Fahlman et al. (1996) presented photometric datasets of M 55 that have been mainly used to study the age and the tidal extension of the Sagittarius dwarf galaxy. Mandushev et al. (1996) published the first deep (down to $V \sim 24.5$) photometry of the cluster.

References

Alcaino G., Liller W., 1986a, A&A 161, 61
Alcaino G., Liller W., 1986b, AJ 91, 303
Alcaino G., Liller W., 1987a, ApJ 319, 304
Alcaino G., Liller W., 1987b, AJ 94, 1585
Alcaino G., Buonanno R., Caloi V., et al., 1987, AJ 94, 917
Alcaino G., Liller W., Alvarado F., 1989, A&A 216, 68
Alcaino G., Liller W., Alvarado F., Wenderoth E., 1990a, AJ 99, 817
Alcaino G., Liller W., Alvarado F., Wenderoth E., 1990b, A&AS 83, 269
Alcaino G., Liller W., Alvarado F., Wenderoth E., 1990c, ApJS 72, 693
Alcaino G., Liller W., Alvarado F., Wenderoth E., 1990d, AJ 99, 1831
Alcaino G., Liller W., Alvarado F., Wenderoth E., 1991, AJ 102, 159
Alcaino G., Liller W., Alvarado F., Wenderoth E., 1992, AJ 104, 1850
Alcaino G., Liller W., Alvarado F., Wenderoth E., 1994, AJ 107, 230
Alcaino G., Liller W., Alvarado F., et al., 1997a, AJ 114, 189
Alcaino G., Liller W., Alvarado F., et al., 1997b, AJ 114, 1067
Alcaino G., Liller W., Alvarado F., et al., 1997c, AJ 114, 2638
Alcaino G., Liller W., Alvarado F., et al., 1998, AJ 116, 2415
Alcaino G., Liller W., Alvarado F., et al., 1999, A&AS 136, 461
Anthony-Twarog B.J., Twarog B.A., Suntzeff N.B., 1992, AJ 103, 1264
Anthony-Twarog B.J., Twarog B.A., Craig J., 1995, PASP 107, 32
Armandroff T., 1988, AJ 96, 588
Auriere M., Ortolani S., Lauzeral C., 1990, Nat 344, 638
Bolte M., 1989, AJ 97, 1688
Bolte M., Marleau F., 1989, PASP 101, 1088
Brewer J.P., Fahlman G.G., Richer H.B., Searle L., Thompson I., 1993, AJ 105, 2158
Brocato E., Buonanno R., Malakhova Y., Piersimoni A.M., 1996, A&A 311, 778
Brocato E., Castellani, V., Scotti G.A., Saviane I., Piotto G., Ferraro F.R., 1998, A&A 335, 929
Buonanno R., Corsi C.E., Iannicola G., Fusi Pecci F., 1986, A&A 159 189
Buonanno R., Corsi C.E., Fusi Pecci F., 1989, A&A 216, 80
Buonanno R., Corsi C.E., Pulone L., Fusi Pecci F., Bellazzini M., 1998, A&A 333, 505

Burgarella D., Paresce F., Meylan G., et al., 1994, A&A 287, 769
Byun Y-L., Lee Y-W., 1993, ASP Conf Ser 13, 243
Caloi V., Castellani V., Piccolo F., 1987, A&AS 67, 181
Carretta E., Gratton R., 1997, A&AS 121, 95
Catelan, M., Borissova, J., Sweigart A.V., Spassova N., 1998, ApJ 494, 265
Chaboyer B., Demarque P., Sarajedini A., 1996, ApJ 459, 558
Cool A.M., Grindlay J.E., Cohn H.N., Lugger P.M., Slavin S.D., 1995, ApJ 439, 695
Cool A.M., Piotto G., King I.R., 1996, ApJ 468, 655
Covino S., Ortolani S., 1997, A&A 318, 40
Davidge T.J., Harris W.E., 1996, ApJ 462, 255
Davidge T.J., Harris W.E., Bridges T.J., Hanes D.A., 1992, ApJS 81, 251
Davidge T.J., Cote P., Harris W.E., 1996, ApJ 468, 641
De Marchi G., Paresce F., 1994, A&A 281, L13
Elson R.A.W., Gilmore G.F., Santiago B.X., Casertano S., 1995, AJ 110, 682
Fahlman G.G., Mandushev G., Richer H.B., Thompson I., Sivaramakrishnan A., 1996, ApJ 459, L65
Ferraro F.R., Clementini G., Fusi Pecci F., Buonanno R., Alcaino G., 1990, A&AS 84, 59
Ferraro F.R., Fusi Pecci F., Montegriffo P., Origlia L., Testa V., 1991, A&A 298, 461
Ferraro F.R., Fusi Pecci F, Buonanno R., 1992, MNRAS 256, 376
Ferraro F.R., Clementini G., Fusi Pecci F., Sortino R., Buonanno R., 1993a, MNRAS 256, 391
Ferraro F.R., Clementini G., Fusi Pecci F., Vitiello E., Buonanno R., 1993b, MNRAS 264, 273
Ferraro F.R., Clementini G., Fusi Pecci, F., Buonanno R., 1995, MNRAS 252, 357
Ferraro F.R., Carretta E., Fusi Pecci F., Zamboni A., 1997, A&A 327, 598
Ferraro F.R., Paltrinieri B., Fusi Pecci F., Rood R.T., Dorman B., 1998, ApJ 500, 311
Friel E.D., Geisler D., 1991, AJ 101, 1338
Fullton L.K., Carney B.W., Olszewski E.W., et al., 1995, AJ 110, 652
Fullton L.K., Carney B.W., 1996, PASP Conf. Ser.,92, 265
Gratton R., Ortolani S., 1986, A&AS 65, 63
Gratton R., Ortolani S., 1987, A&AS 67, 373
Green E.M., Norris J.E., 1990, ApJ 353, L17
Harris W.E., 1996, AJ 112, 1487
Heasley J.N., Janes K.A., Christian C.A., 1983, AJ 91, 1108
Hesser J.E., Harris W.E., Vandenberg D.A., et al., 1987, PASP 99, 739
Ibata R.A., Richer H.B., Fahlman G.G., et al., 1999, ApJS 120, 265
Janes K.A., Heasley J.N., 1988, AJ 95, 762
Johnson J.A., Bolte M., 1998, AJ 115, 693
Kaluzny J., 1997b, A&AS 122, 1
Kaluzny J., Kubiak M., Szymanski M., et al., 1996, A&AS 120, 139
Kaluzny J., Kubiak M., Szymanski M., et al., 1997a, ApJS 122, 471
Kaluzny J., Kubiak M., Szymanski M., et al., 1998, A&AS 128, 19
Kanatas I.N., Griffiths W.K., Dickens R.J., Penny A.J., 1995, MNRAS 272, 265
King I., Sosin C., Cool A.M., 1995, ApJ 452, L33
King I., Anderson J., Cool A.M., Piotto G., 1998, ApJ 492, L37
Kravtsov V., Ipatov A., Samus N., et al., 1997, A&AS 125, 1
Landolt A.U., 1992, AJ 104, 340
Lauzeral C., Ortolani S., Auriere M., Melnick J., 1992, A&A 262, 63
Lauzeral C., Auriere M., Caupinot G., 1993, A&A 274, 214
Lee Y.W., 1990, ApJ 363, 159
Lynga G., 1996, A&AS 115, 297
Malakhova Y.N., Gerashchenko A.N., Kadla Z.I., 1997, Information Bulletin on Variable Stars 4457, 1
Mandushev G.I., Fahlman G.G., Richer H.B., 1996, AJ 112, 1536
Mateo M., Mirabal N., Udalski A., et al., 1996, ApJ 458, L13
McClure R.D., Hesser J.E., Stetson P.B., Stryker L.L., 1985, PASP 97, 665
McClure R.D., VandenBerg D.A., Bell R.A., Hesser J.E., Stetson P.B., 1987, AJ 93, 1144
Noble R.G., Dickens R.J., Buttress J., Griffiths W.K., Penny A.J., 1991, MNRAS 250, 314
Norris J.E., Freeman K.C., Mighell K.J., 1996, ApJ 462, 241
Ortolani S., Barbuy B., Bica E., 1999, A&AS 136, 237
Penny A.J., 1984, IAU Symp 105, 157
Penny A.J., Dickens R.J., 1986, MNRAS 220, 845
Piotto G., Zoccali M., 1999, A&A 345, 485
Piotto G., Zoccali M., King I.R., et al., 1999, AJ 117, 264
Pulone L., De Marchi G., Paresce F., 1999, A&A 342, 440
Renzini A., Bragaglia A., Ferraro F.R., et al., 1996, ApJ 465, L23
Rich E.M., Sosin C., Djorgovski S.G., et al., 1997, ApJ 484, L25
Richer H.B., Harris W.E., Fahlman G.G., et al., 1996, ApJ 463, 602
Richtler T., Grebel E.K., Seggewiss W., 1994, A&A 290, 412
Rosenberg A., Saviane I., Piotto G., Aparicio A., Zaggia S., 1998, AJ 115, 648
Rosenberg A., Saviane I., Piotto G., Aparicio A., 1999, AJ 118, 2306 (Paper III)
Rosenberg A., Aparicio A., Saviane I., Piotto G., 2000, A&AS submitted (Paper II)
Rubenstein E.P., Baylin C.D., 1997, ApJ 474, 701
Rutledge G.A., Hesser J.E., Stetson P.B., 1997, PASP 109, 907
Salaris M., Weiss A., 1998, A&A 335, 943
Salaris M., Degl'Innocenti S., Weiss A., 1997, ApJ 479, 665
Samus N., Kravtsov V., Ipatov A., et al., 1996, A&AS 119, 191
Sarajedini A., 1992, AJ 104, 178
Sarajedini A., Da Costa G.S., 1991, AJ 102, 628
Sarajedini A., Demarque P., 1990, ApJ 365, 219
Sarajedini A., Norris J.E., 1994, AJ 93, 161
Saviane I., Piotto G., Fagotto F., et al., 1998, A&A 333, 479
Saviane I., Rosenberg A., Piotto G., Aparicio A., 2000, A&A in press (Paper IV)
Sosin C., King I.R., 1995, AJ 109, 639
Sosin C., Dorman B., Djorgovski S.G., et al., 1997b, ApJ 480, L35
Sosin C., Piotto G., Djorgovski S.G., et al., 1997a, in "Advances in Stellar Evolution", eds. Rood and Renzini, p. 92
Stetson P.B., 1987, PASP 99, 191
Stetson P.B., 1994, PASP 106, 250
Veronesi C., Zaggia S., Piotto G., Ferraro F.R., Bellazzini M., 1996, ASP Conf. Ser. 92, 301
Walker A.R., 1992, PASP 104, 1063
Walker A.R., 1994, AJ 108, 555
Walker A.R., 1998, AJ 116, 220
Walker A.R., 1999, AJ 118, 432
Zaggia S., Piotto G., Capaccioli M., 1997, A&A 327, 1004
Zinn R., West M.J., 1984, ApJS 55, 45

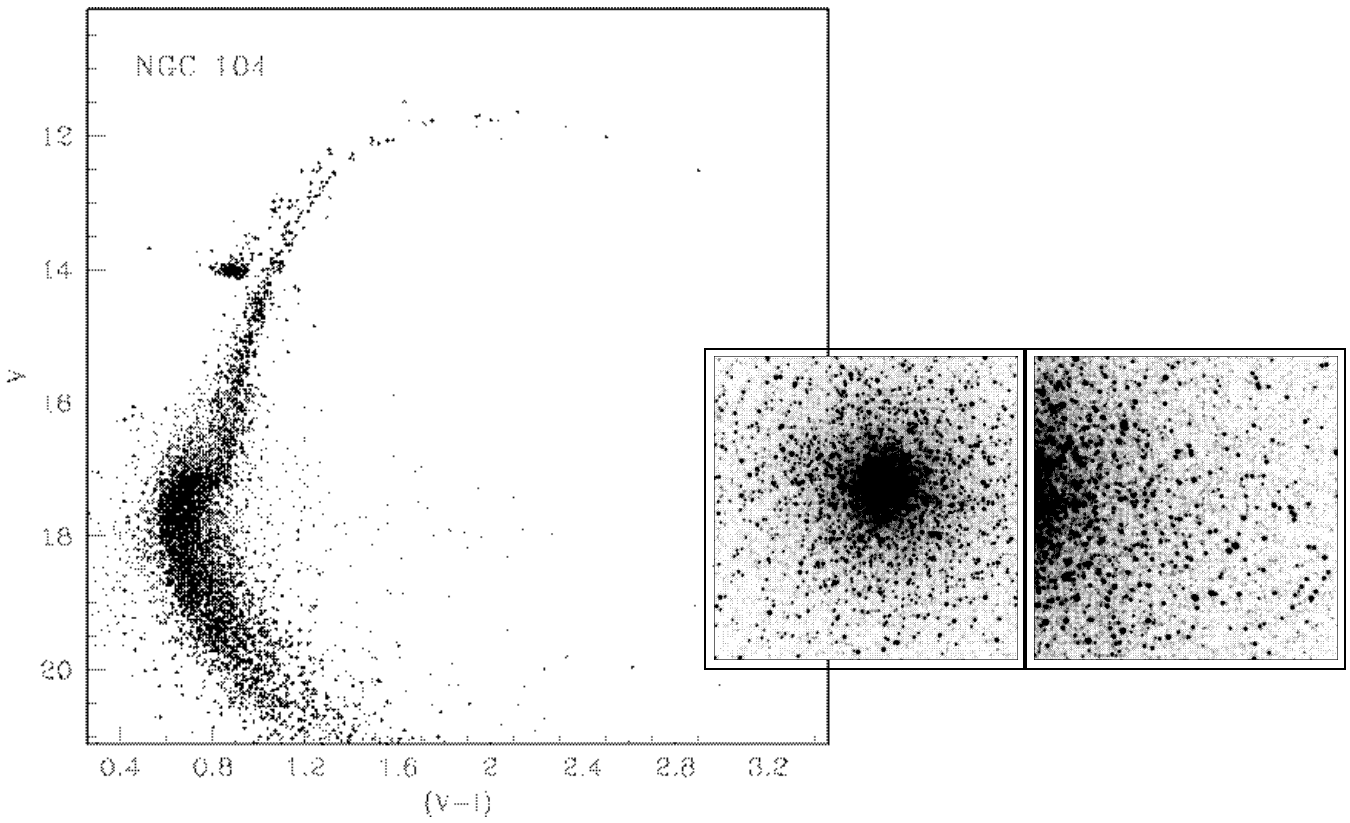

Fig. 4. CMD and covered fields for NGC 104 (47 Tucanae)

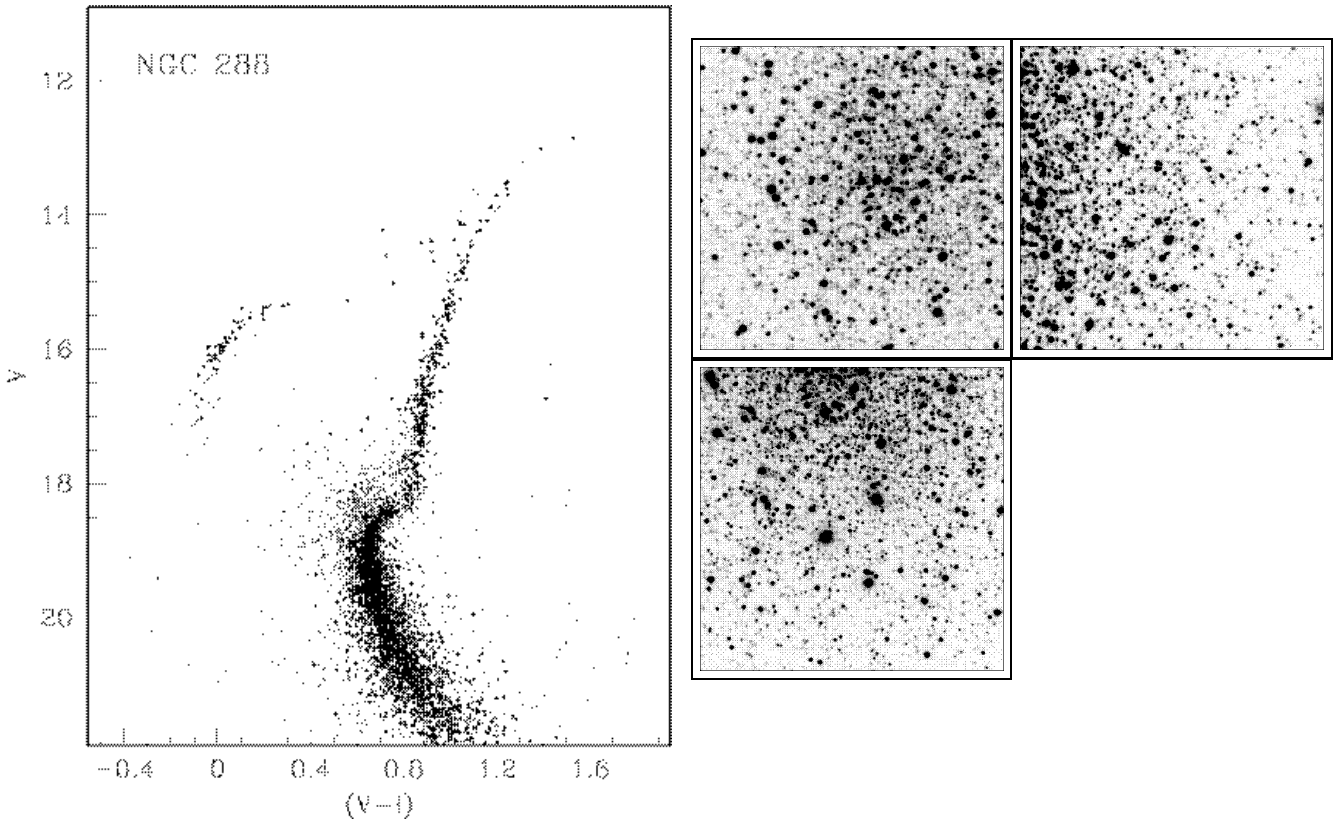

Fig. 5. CMD and covered fields for NGC 288

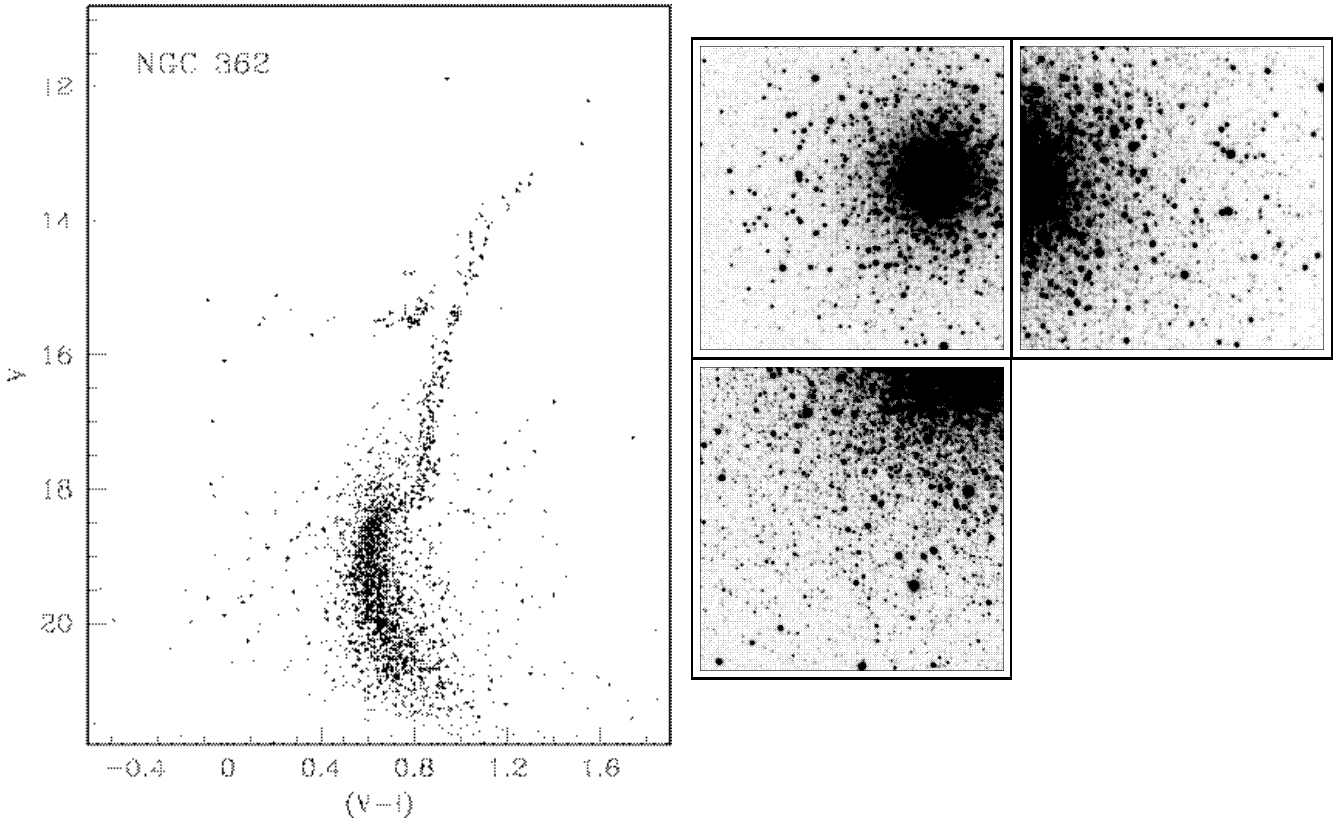

Fig. 6. CMD and covered fields for NGC 362

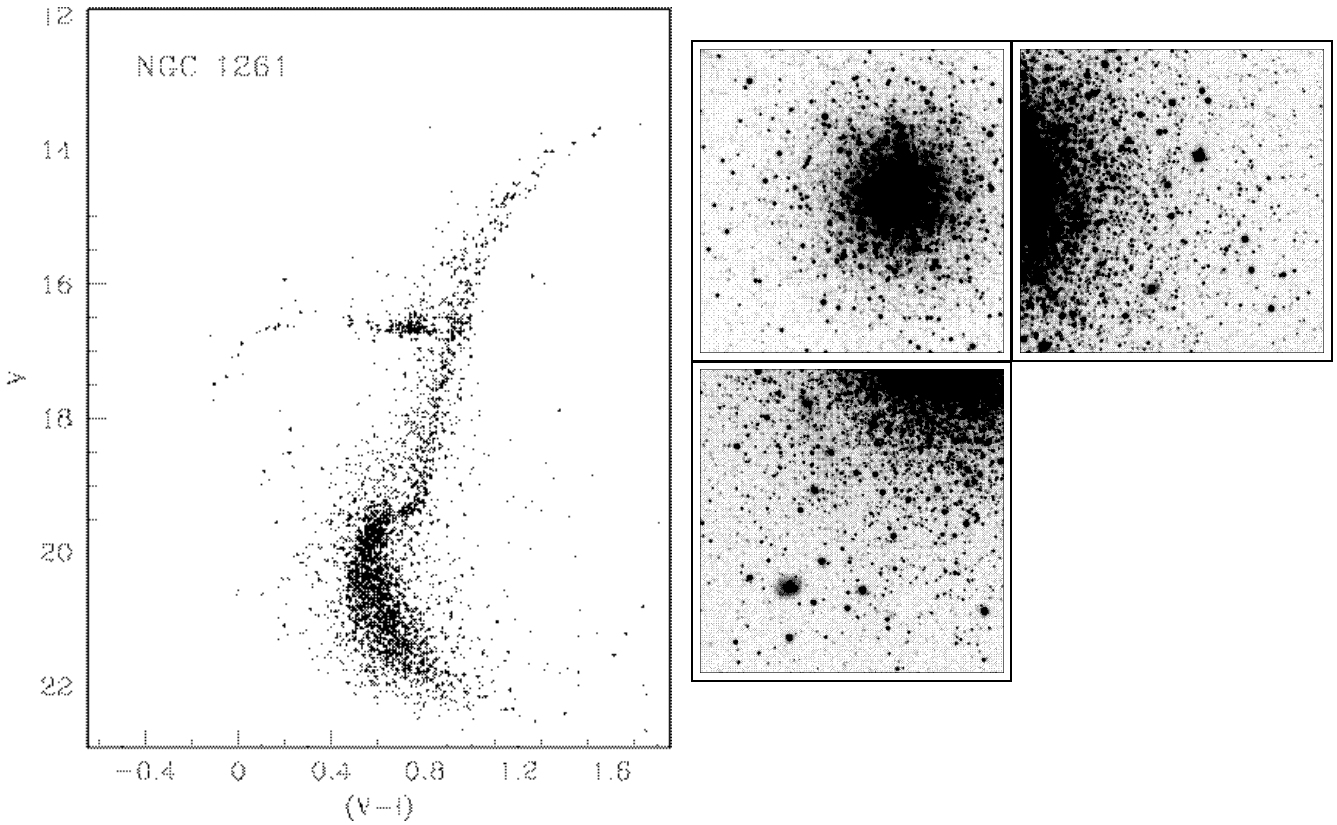

Fig. 7. CMD and covered fields for NGC 1261

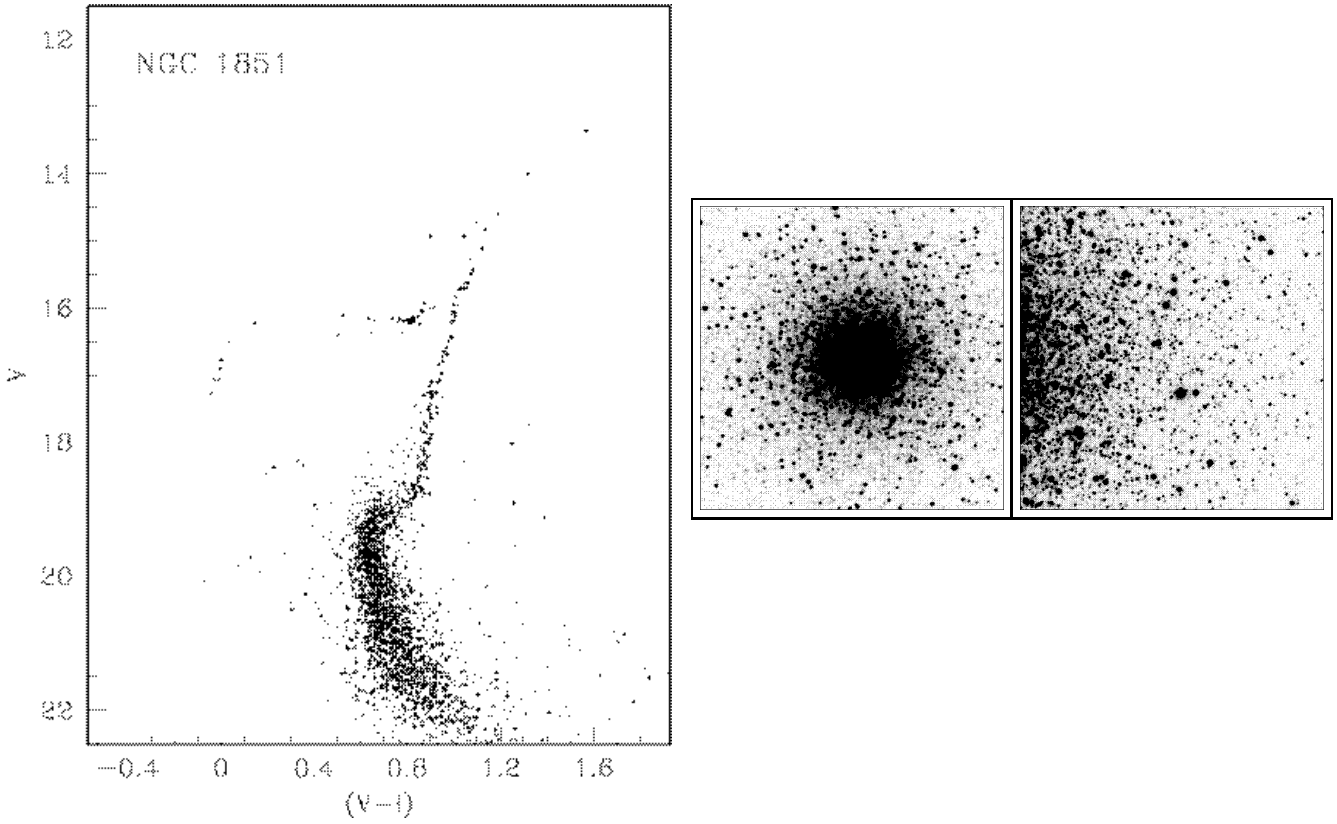

Fig. 8. CMD and covered fields for NGC 1851

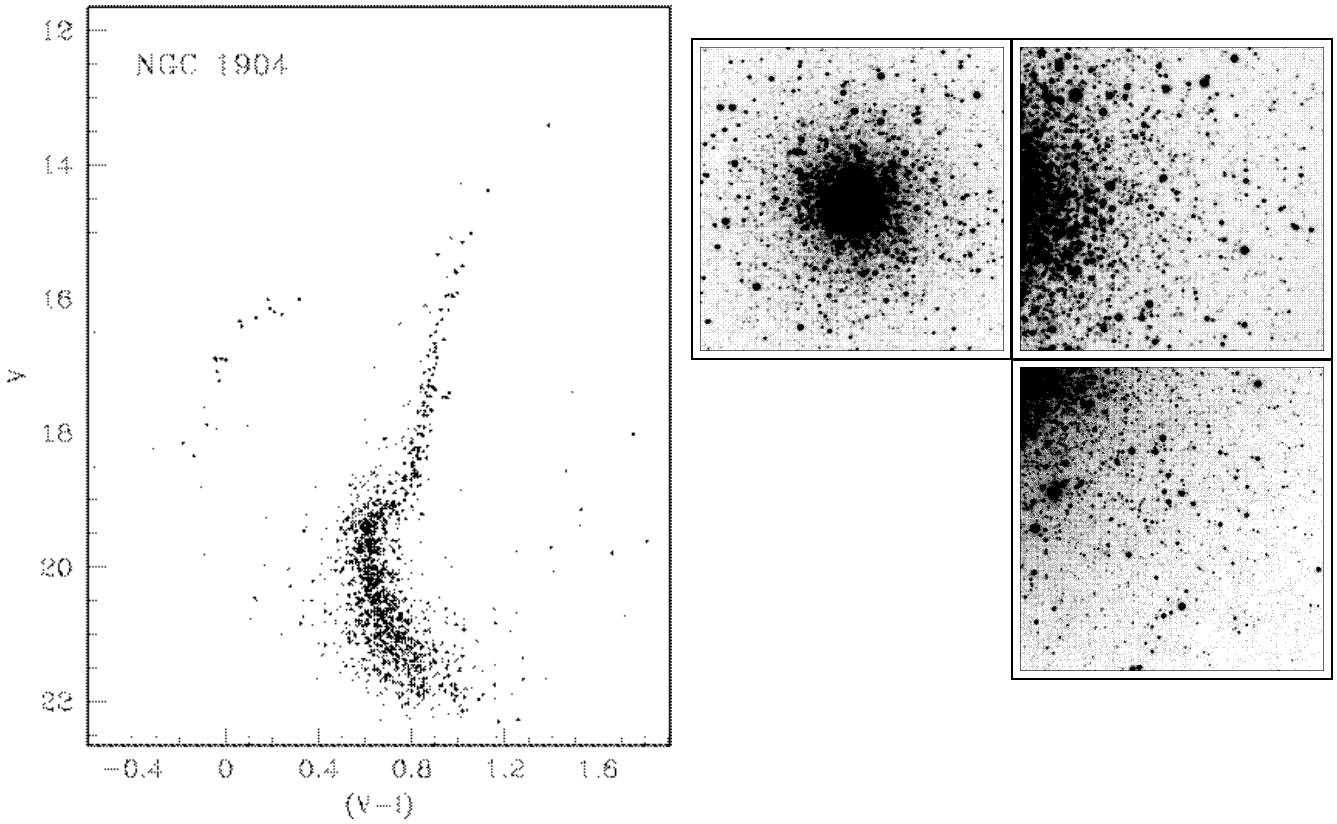

Fig. 9. CMD and covered fields for NGC 1904 (M 79)

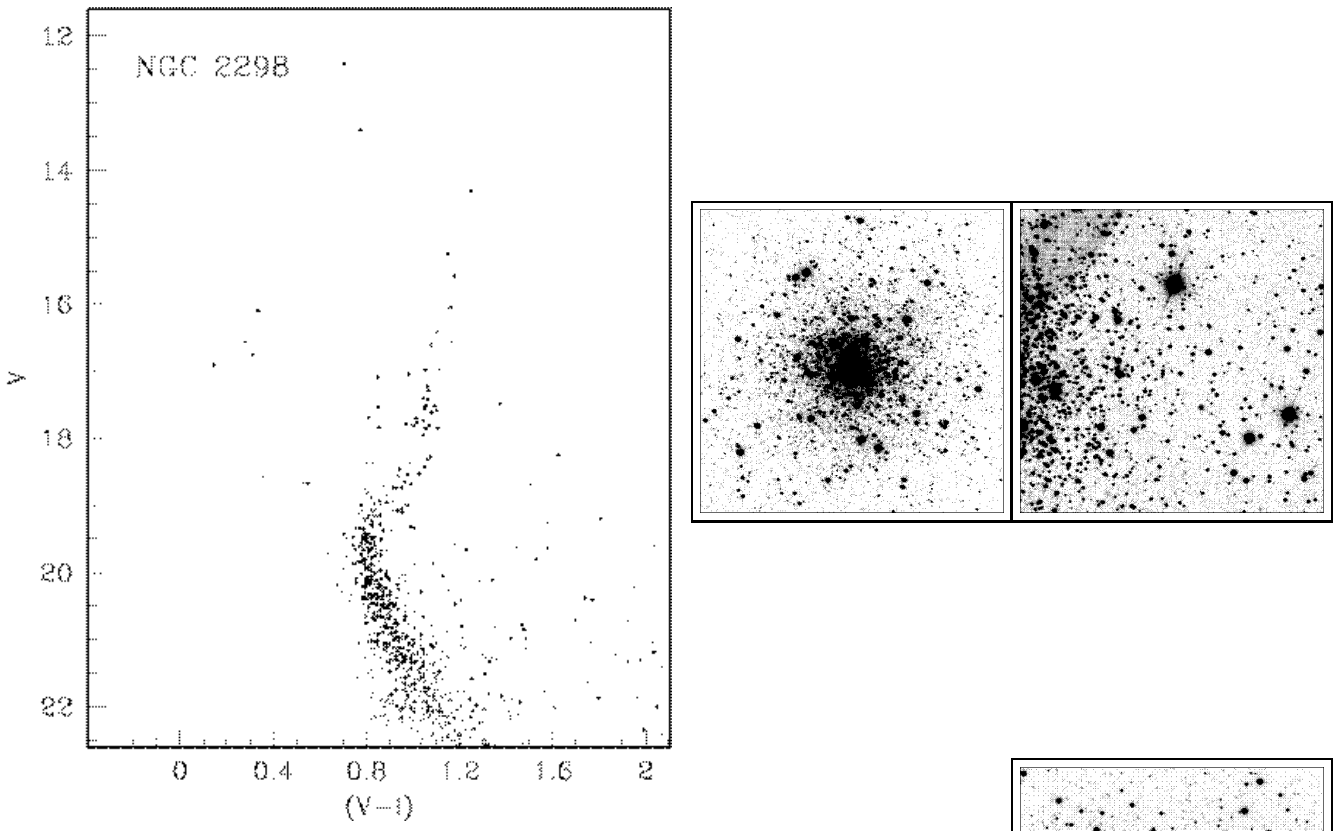

Fig. 10. CMD and covered fields for NGC 2298

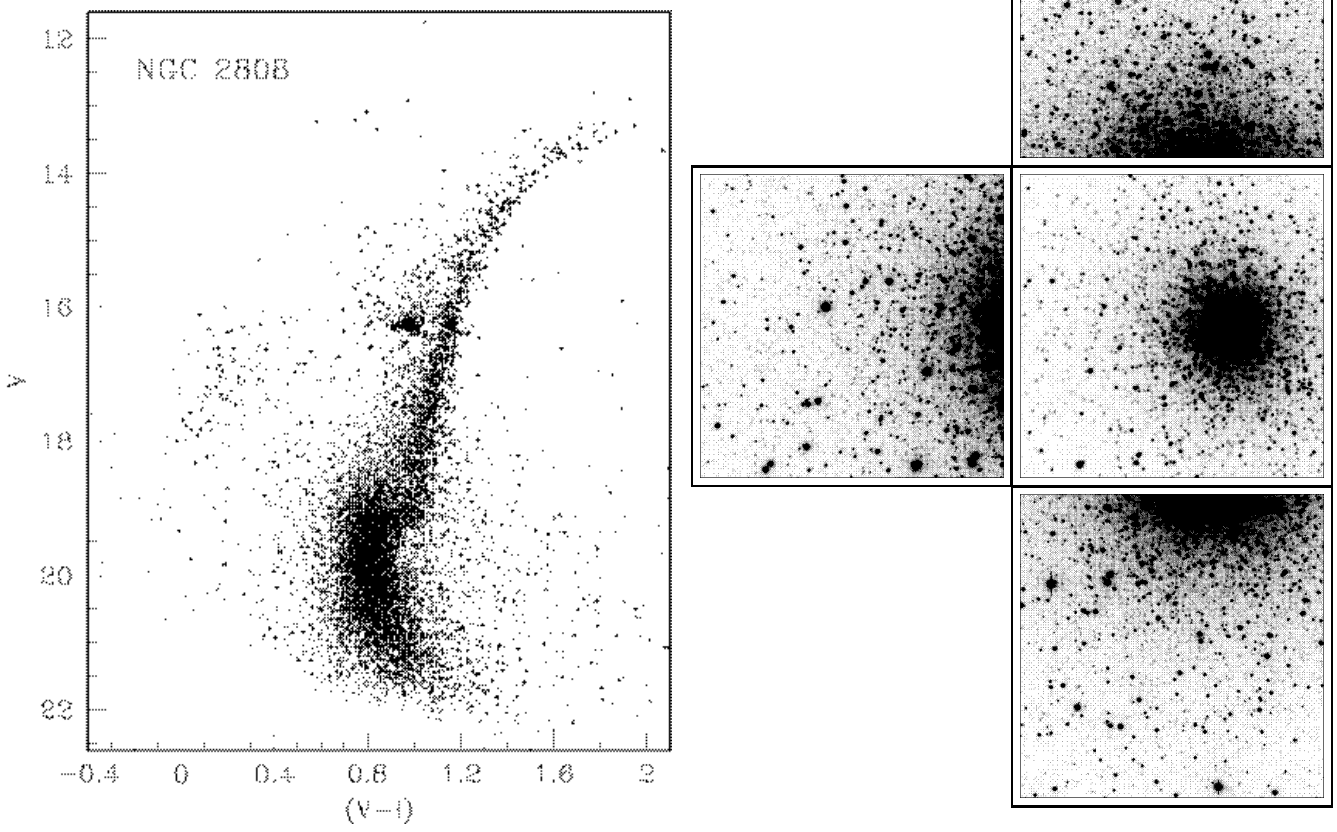

Fig. 11. CMD and covered fields for NGC 2808

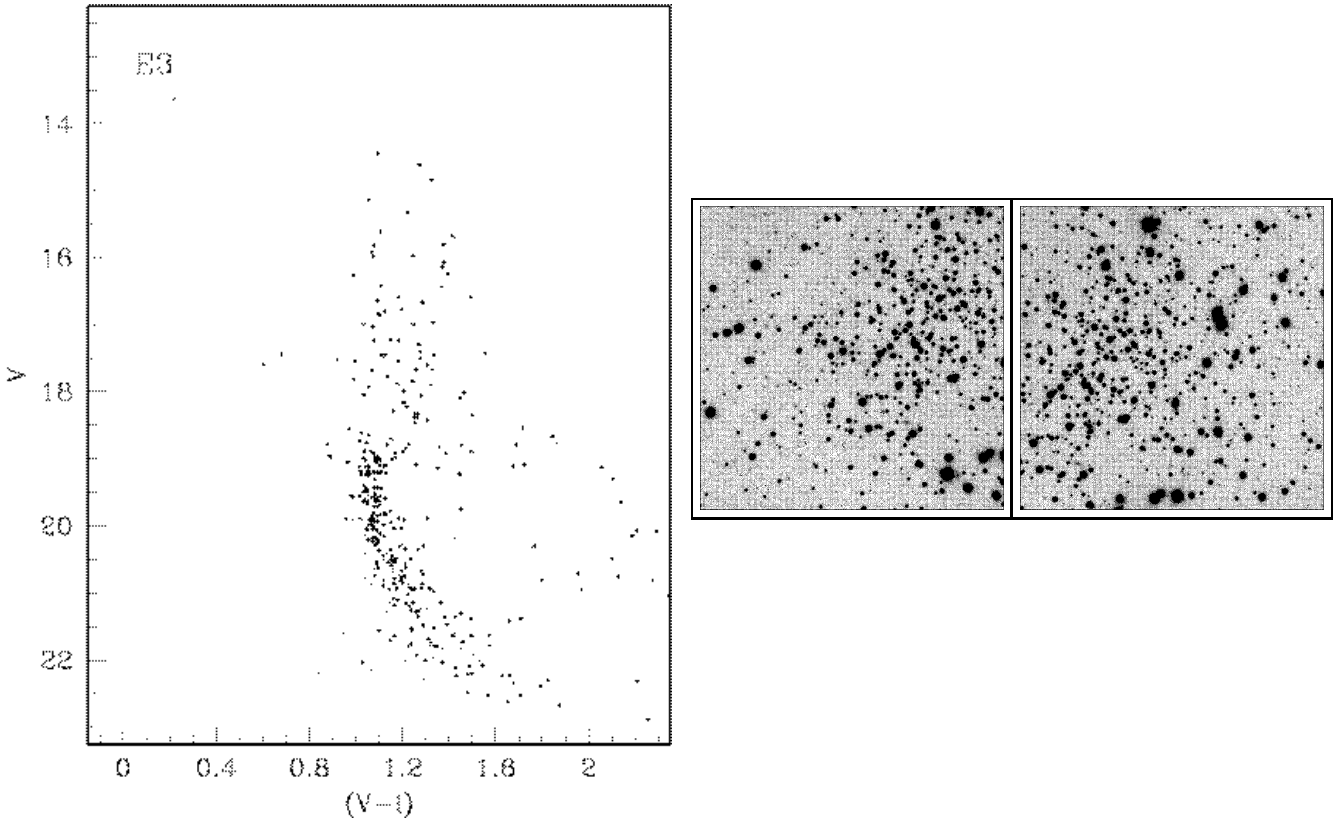

Fig. 12. CMD and covered fields for E3

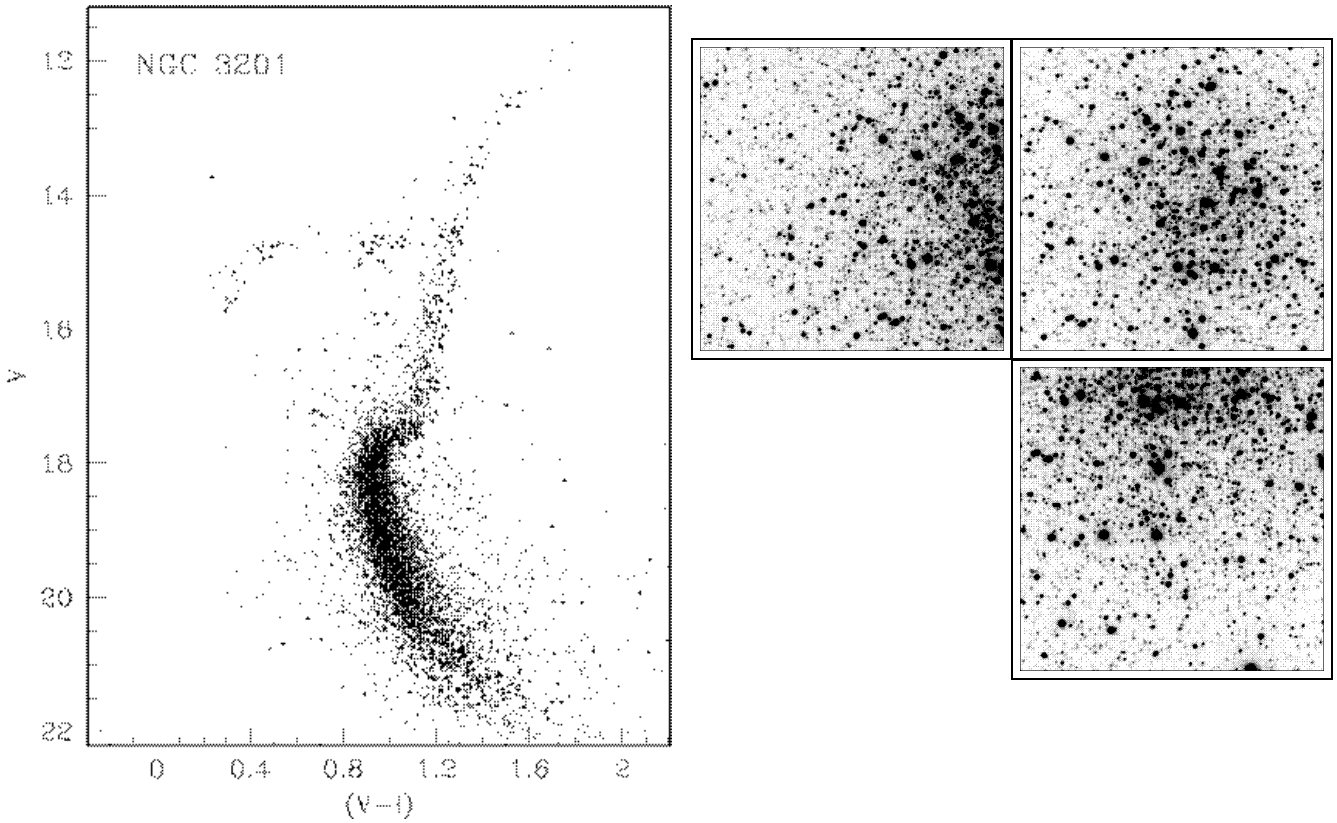

Fig. 13. CMD and covered fields for NGC 3201

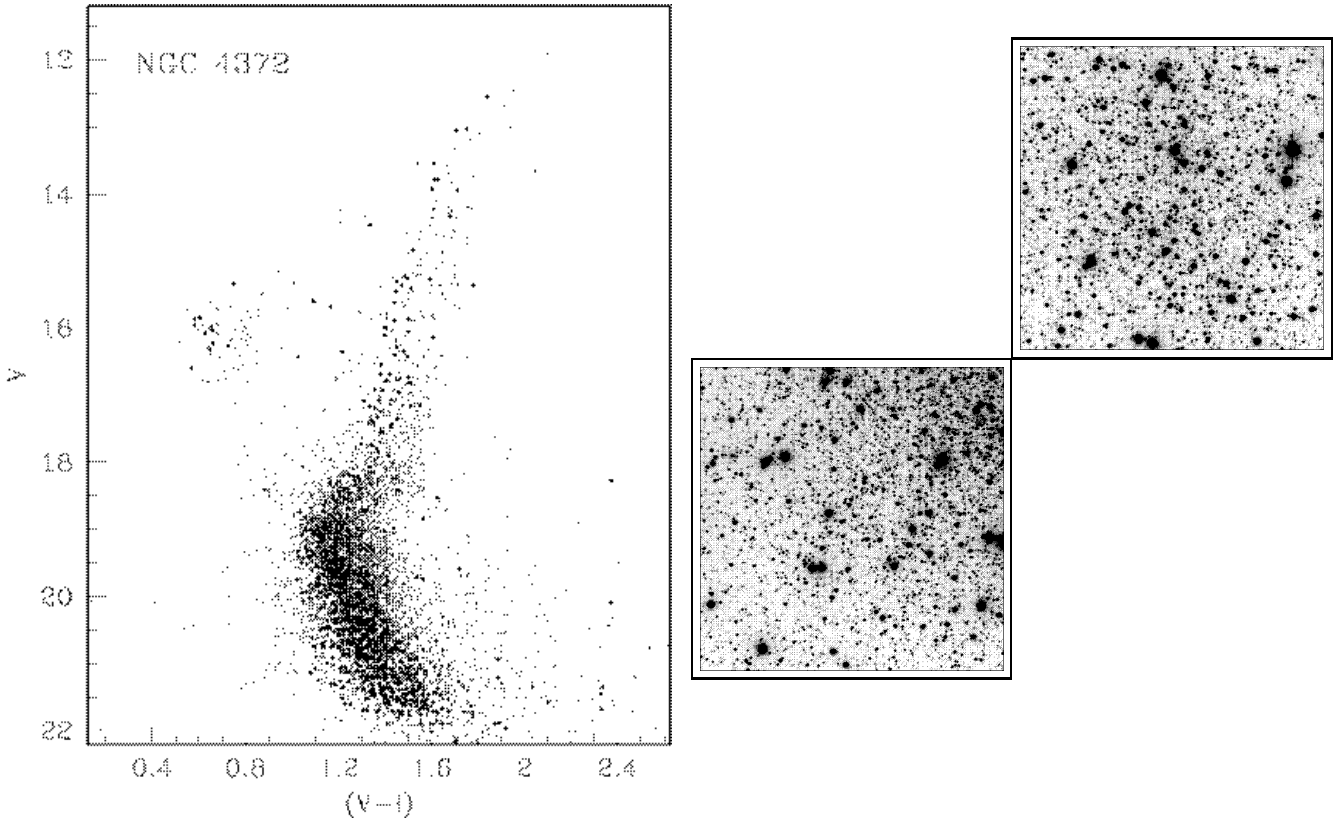

Fig. 14. CMD and covered fields for NGC 4372

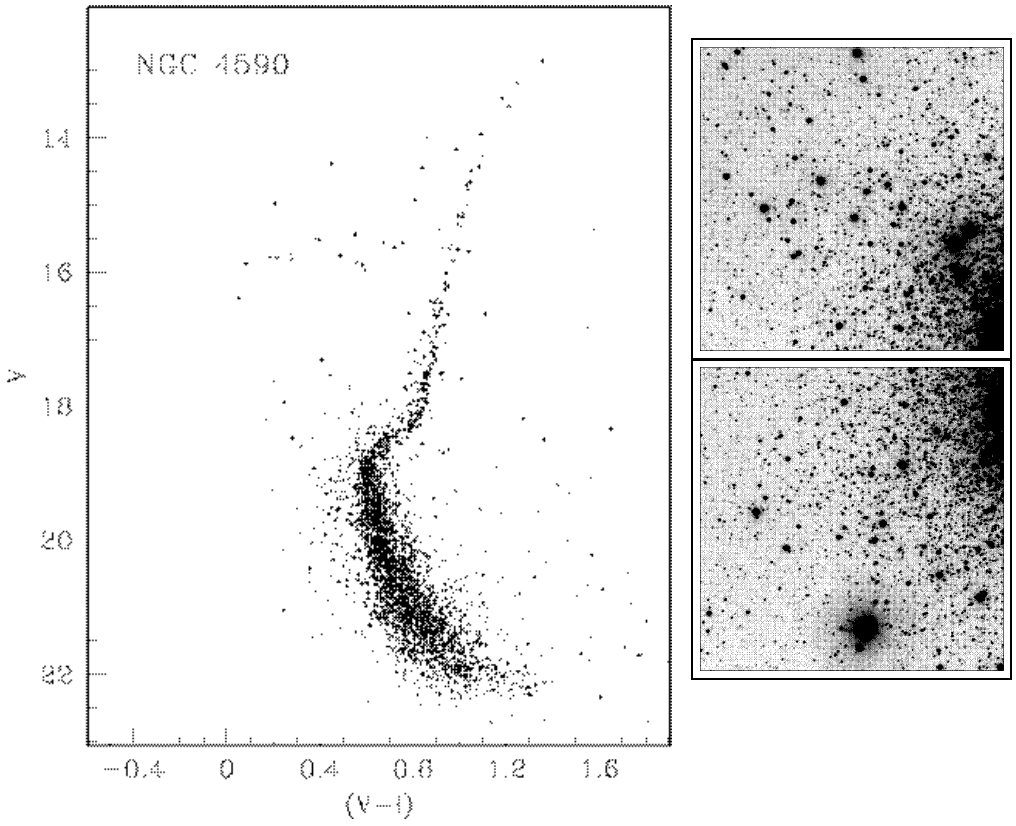

Fig. 15. CMD and covered fields for NGC 4590 (M 68)

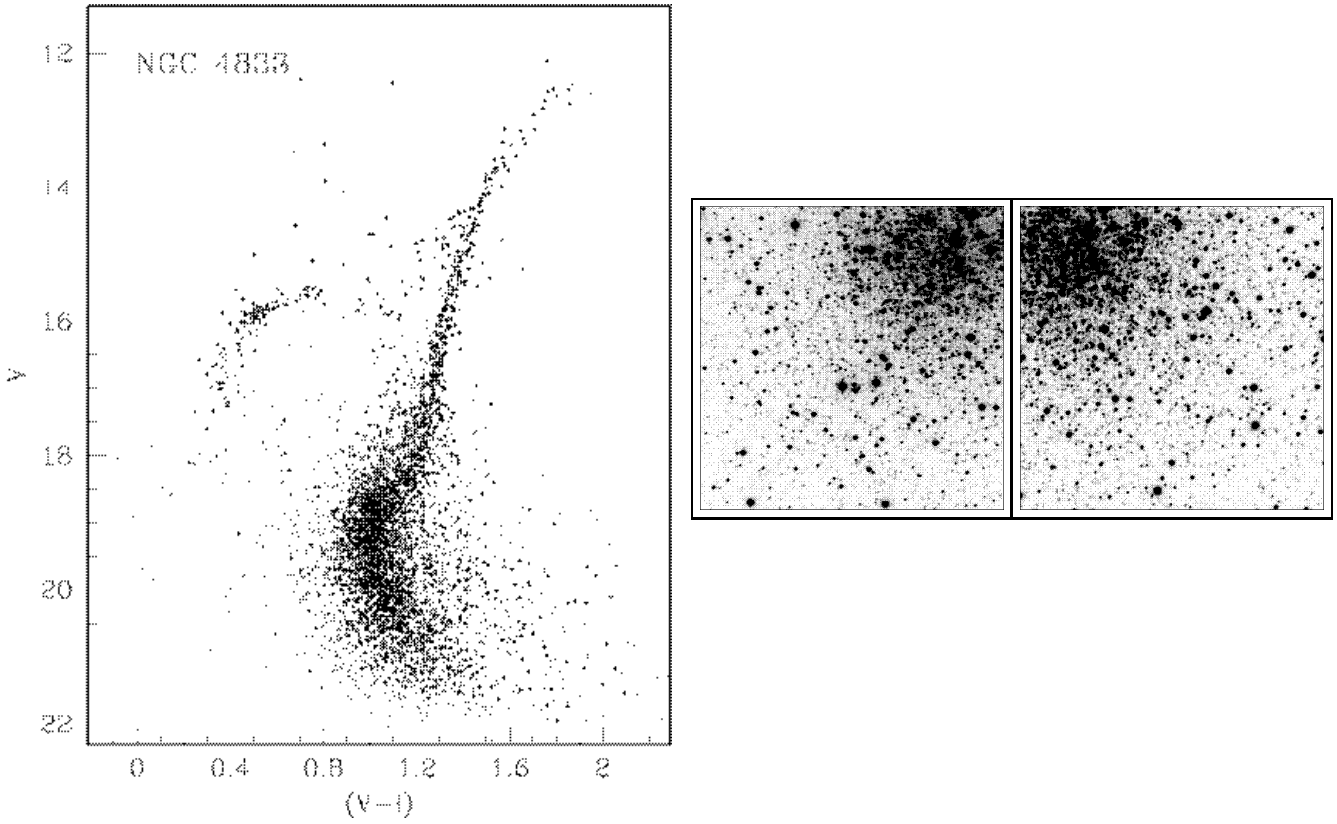

Fig. 16. CMD and covered fields for NGC 4833

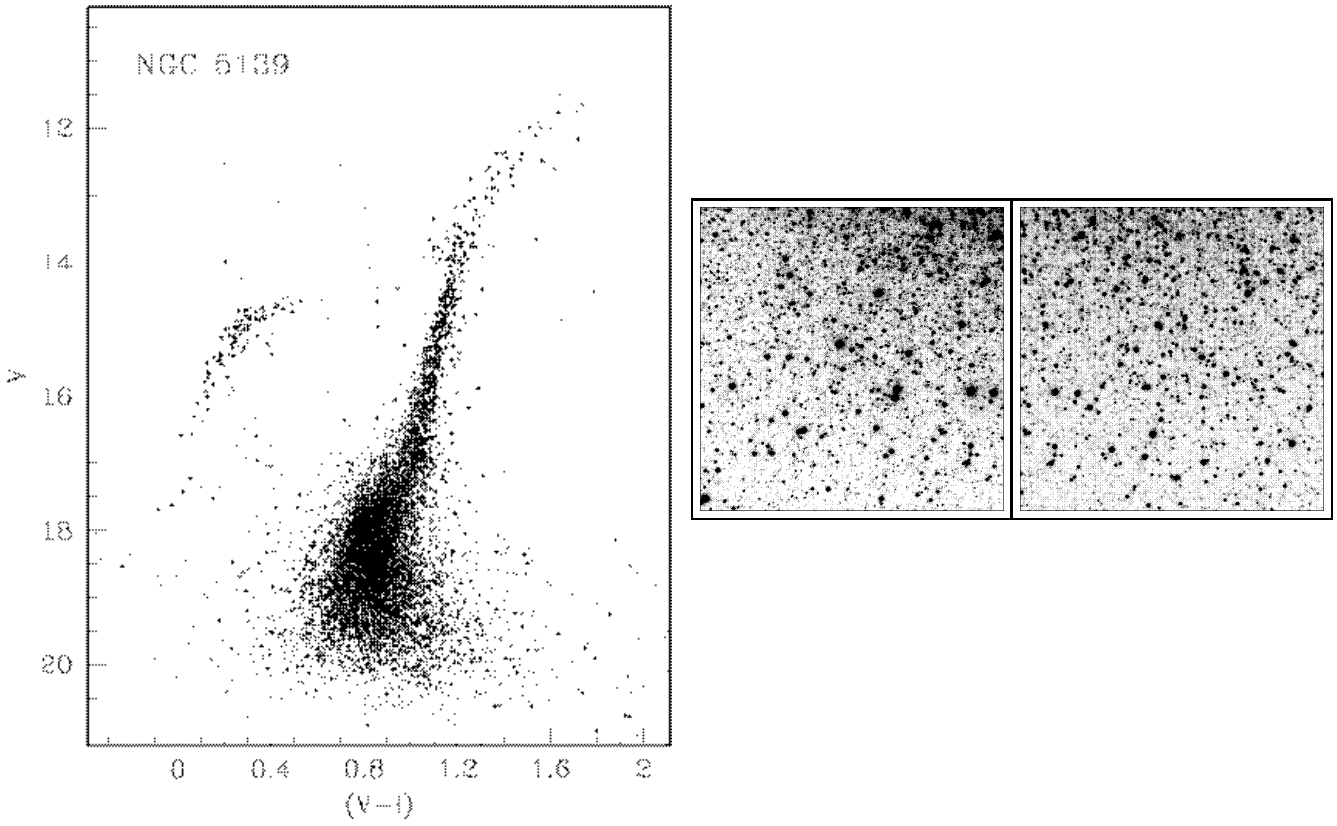

Fig. 17. CMD and covered fields for NGC 5139 (ω Centauri)

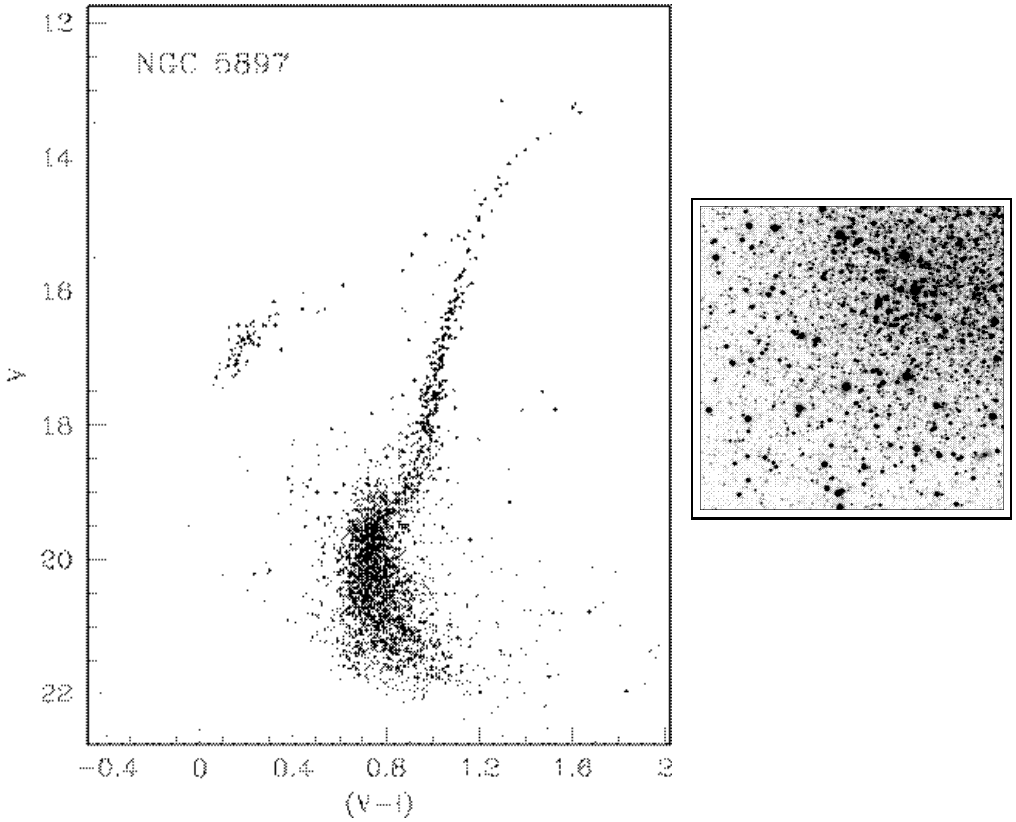

Fig. 18. CMD and covered fields for NGC 5897

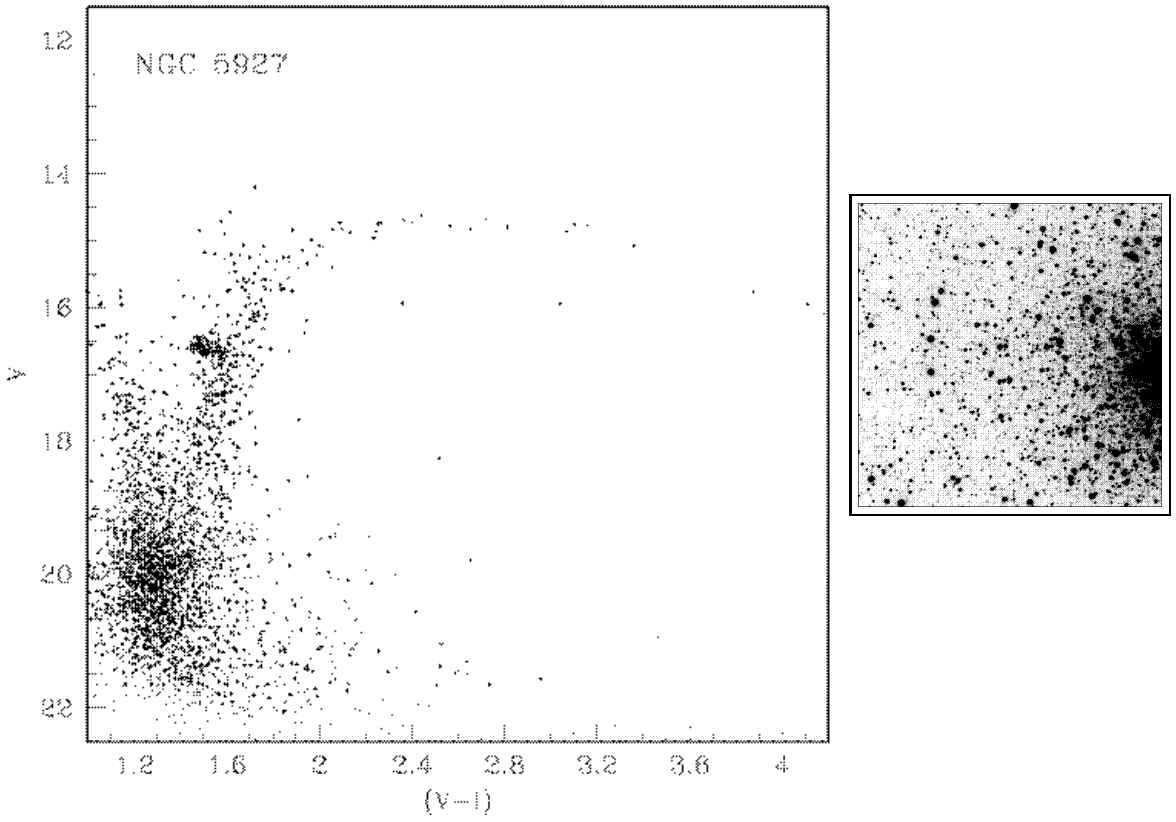

Fig. 19. CMD and covered field for NGC 5927

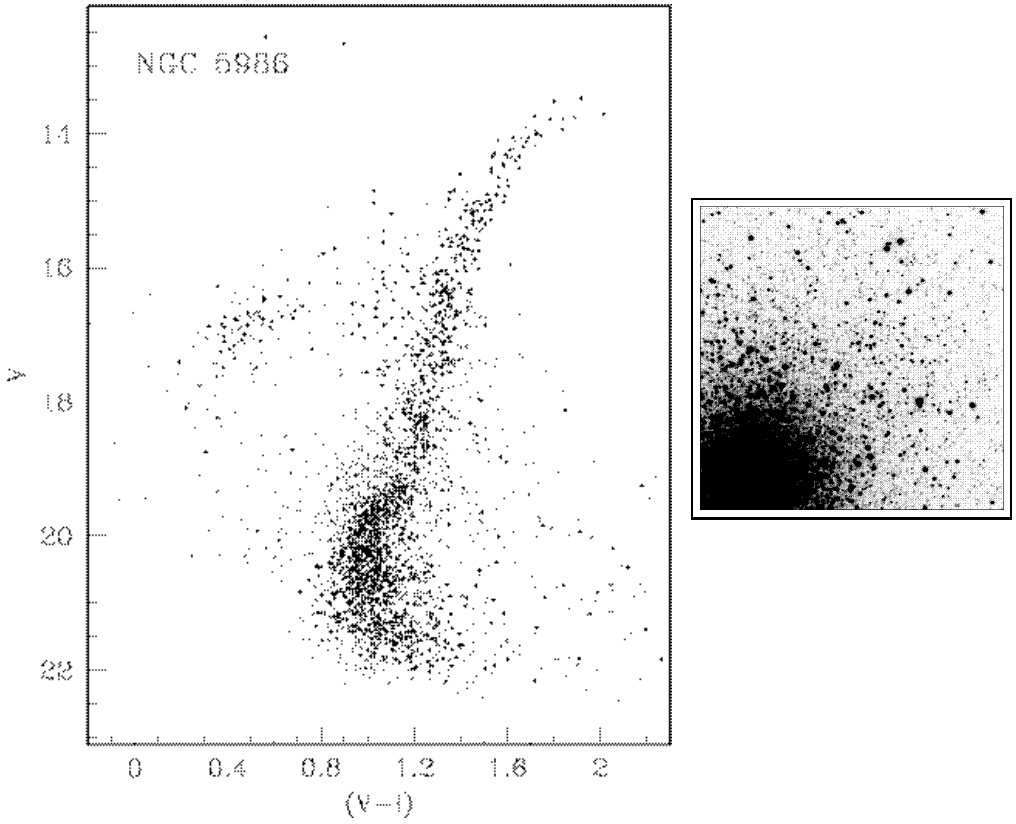

Fig. 20. CMD and covered field for NGC 5986

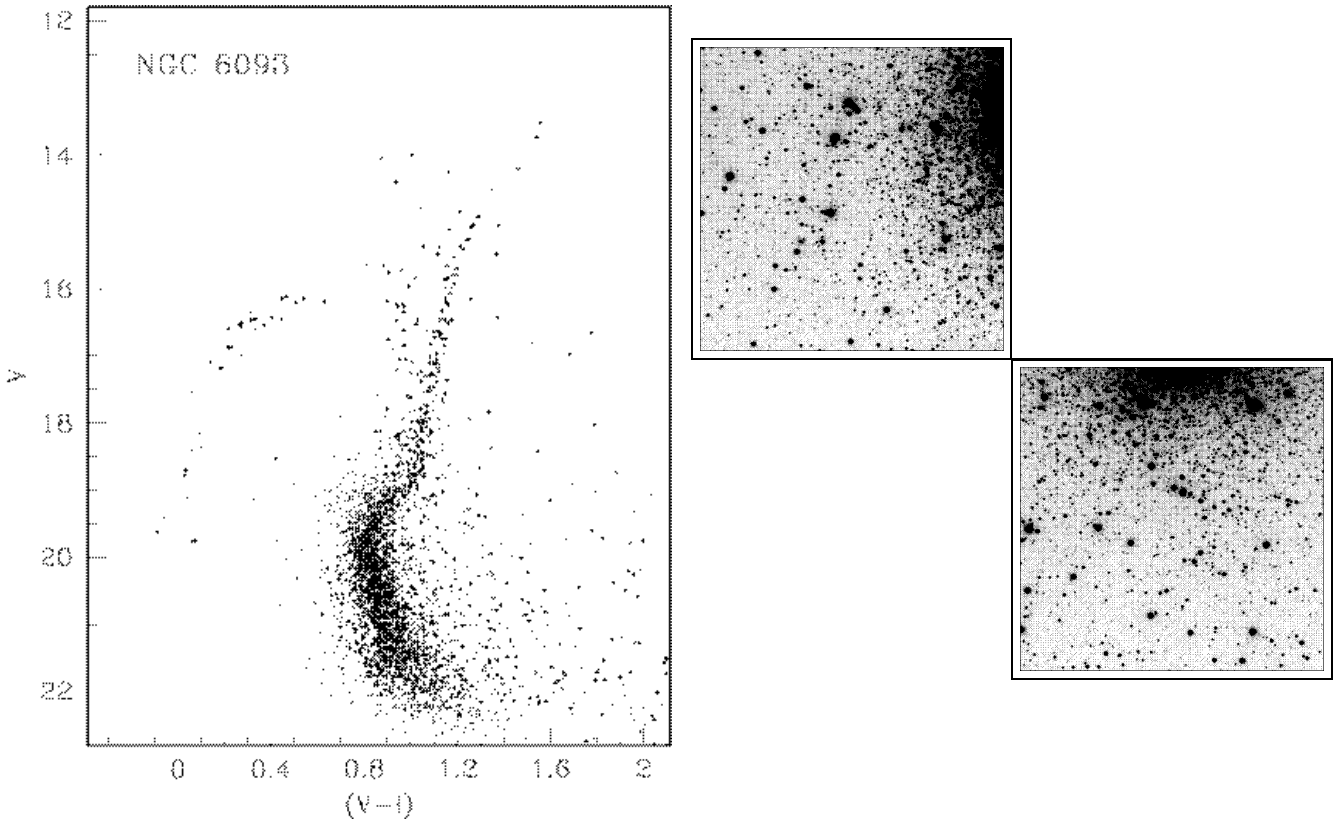

Fig. 21. CMD and covered fields for NGC 6093 (M 80)

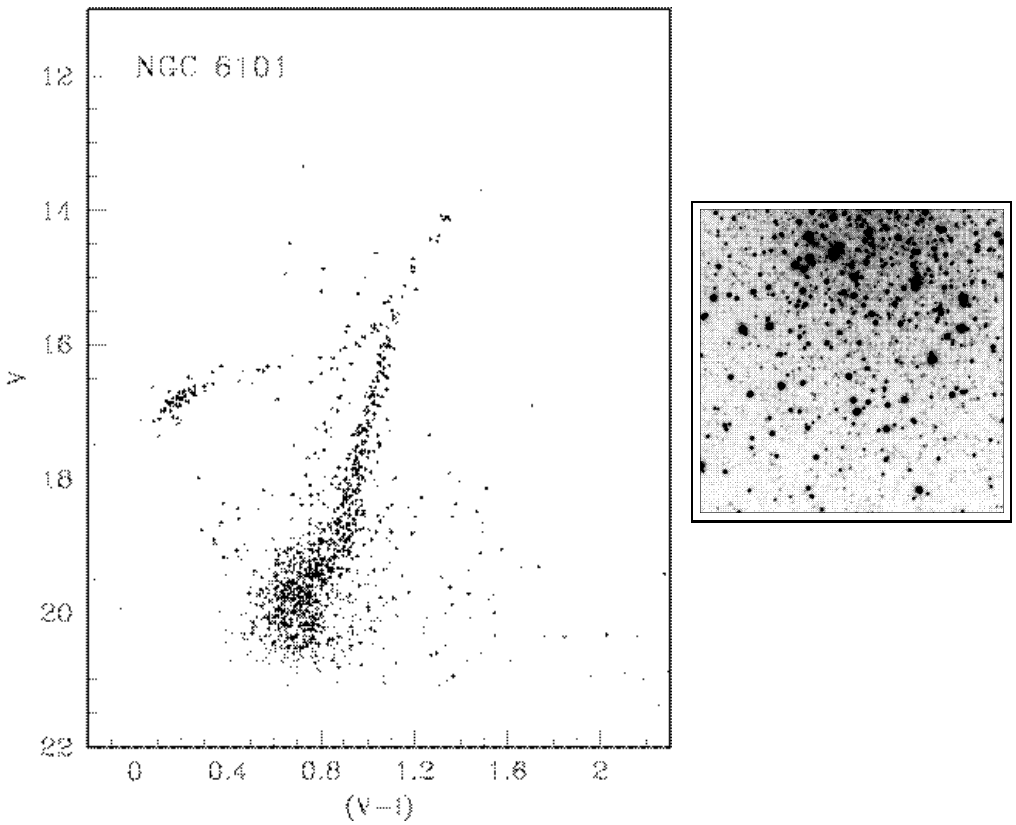

Fig. 22. CMD and covered field for NGC 6101

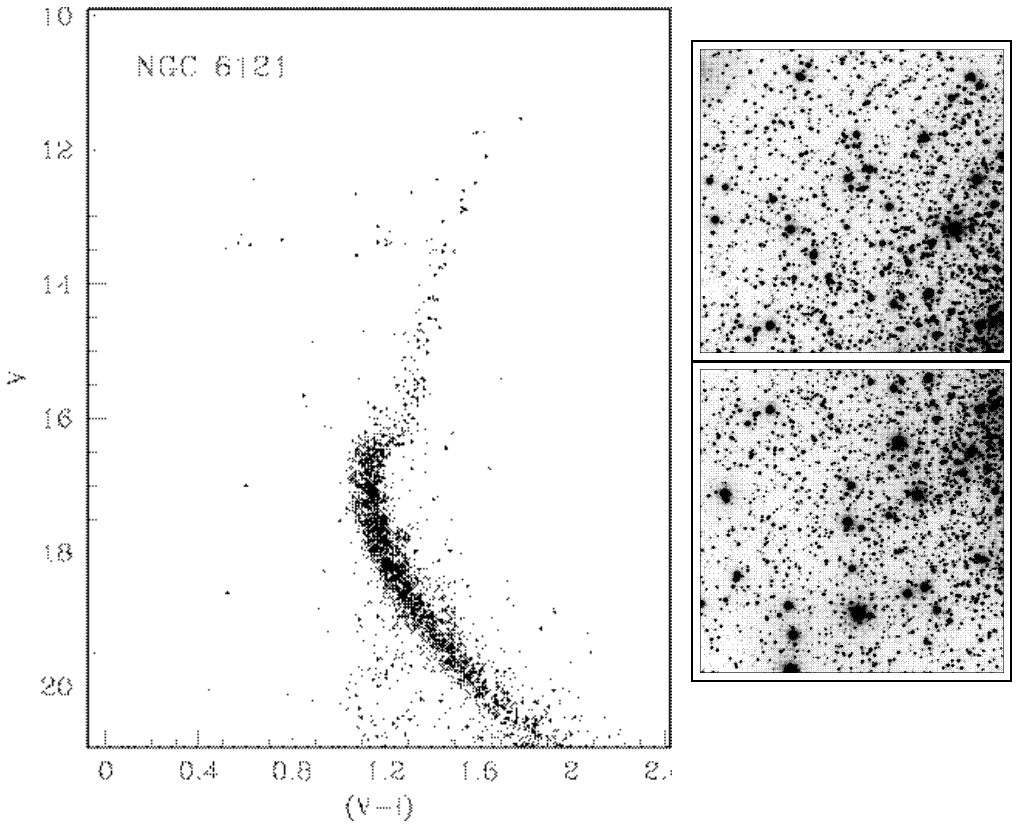

Fig. 23. CMD and covered fields for NGC 6121 (M 4)

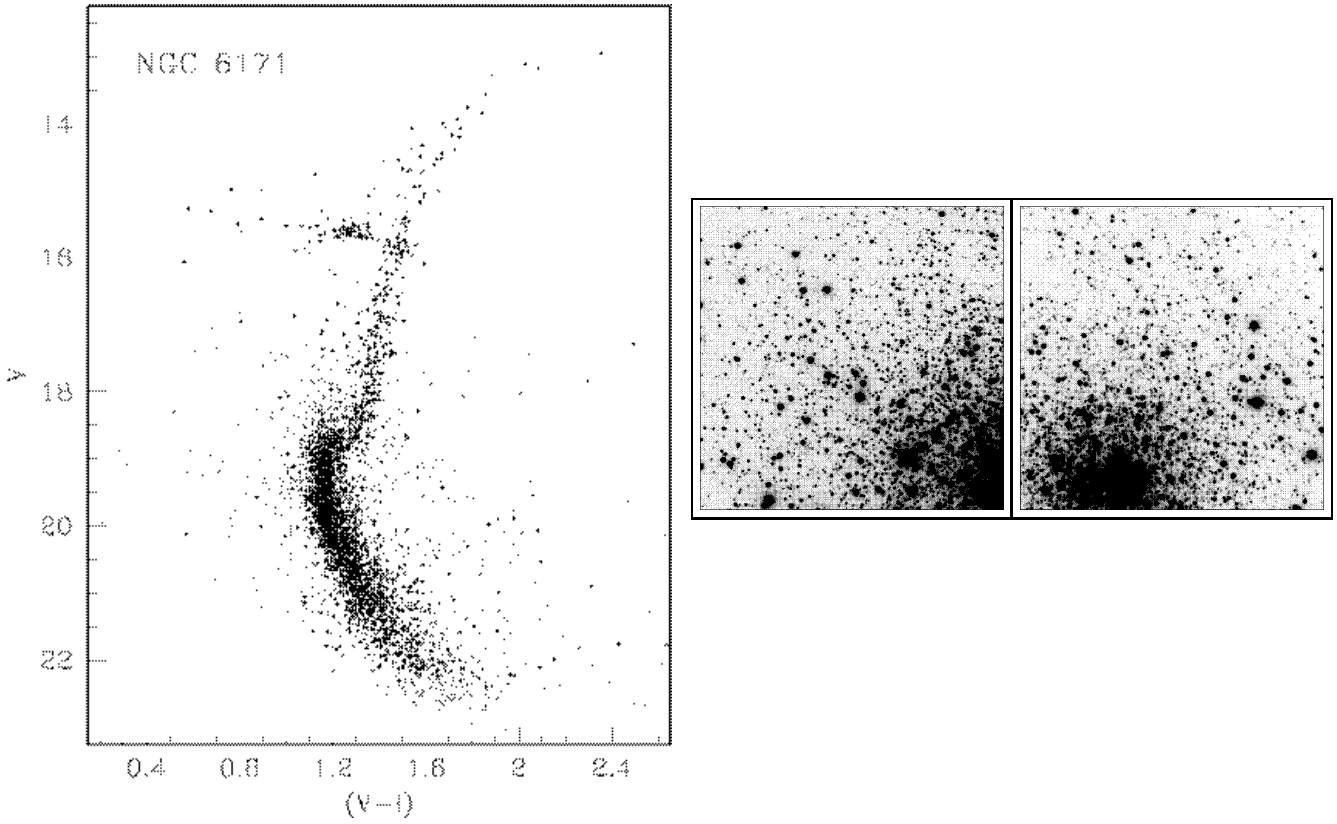

Fig. 24. CMD and covered fields for NGC 6171 (M 107)

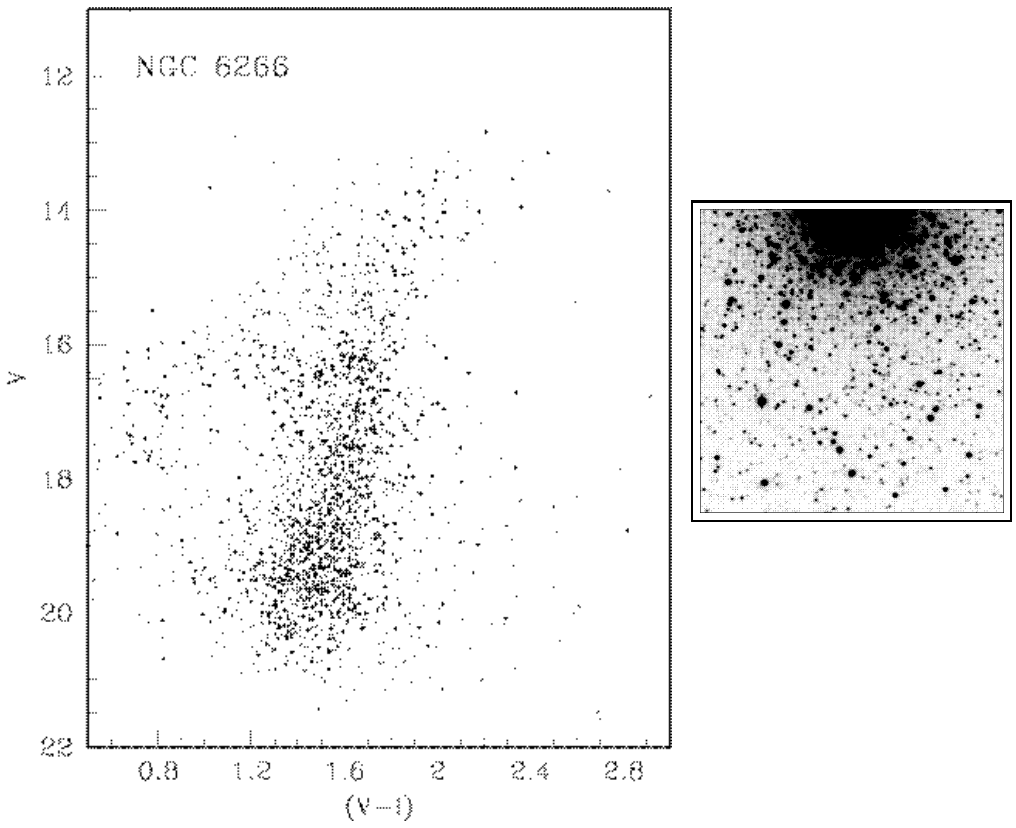

Fig. 25. CMD and covered field for NGC 6266

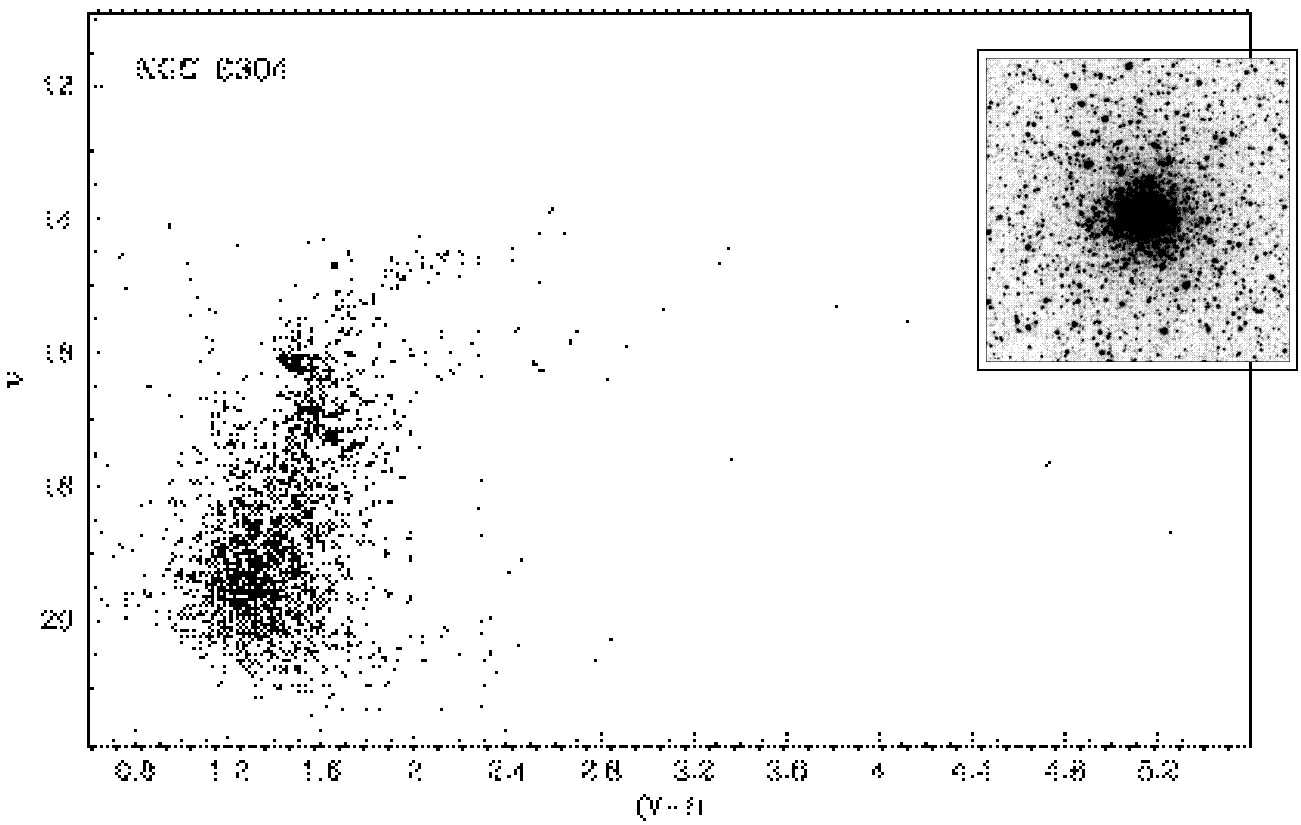

Fig. 26. CMD and covered field for NGC 6304 (M 62)

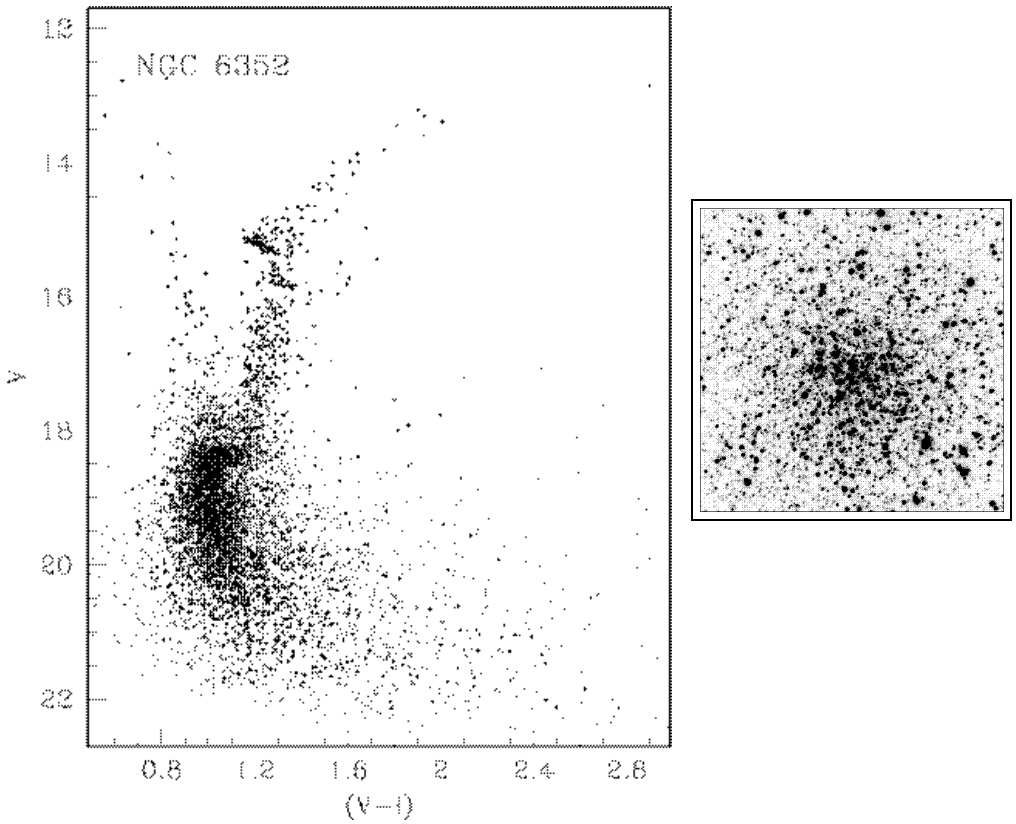

Fig. 27. CMD and covered field for NGC 6352

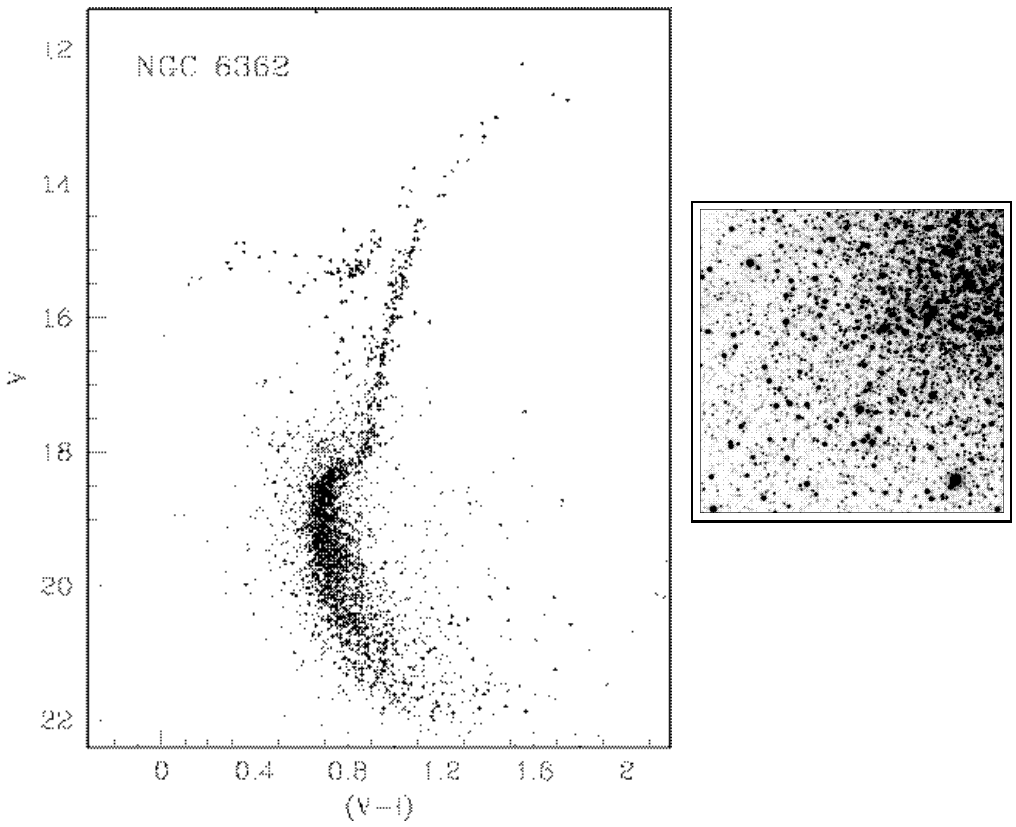

Fig. 28. CMD and covered field for NGC 6362

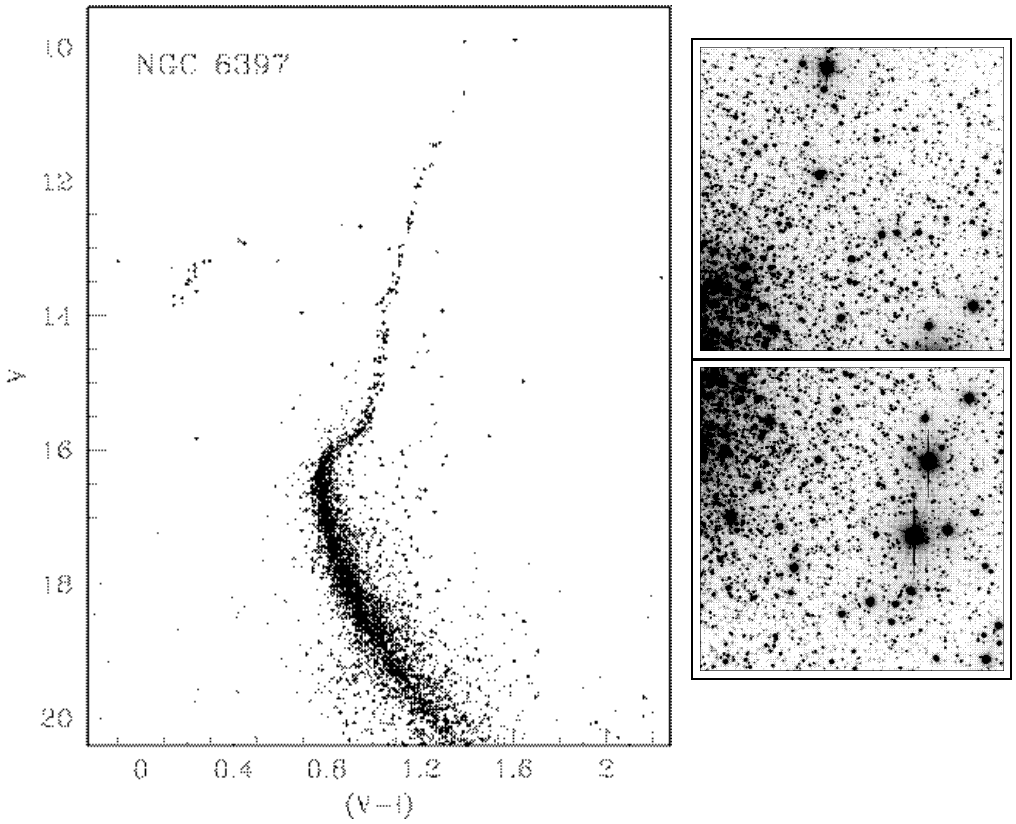

Fig. 29. CMD and covered fields for NGC 6397

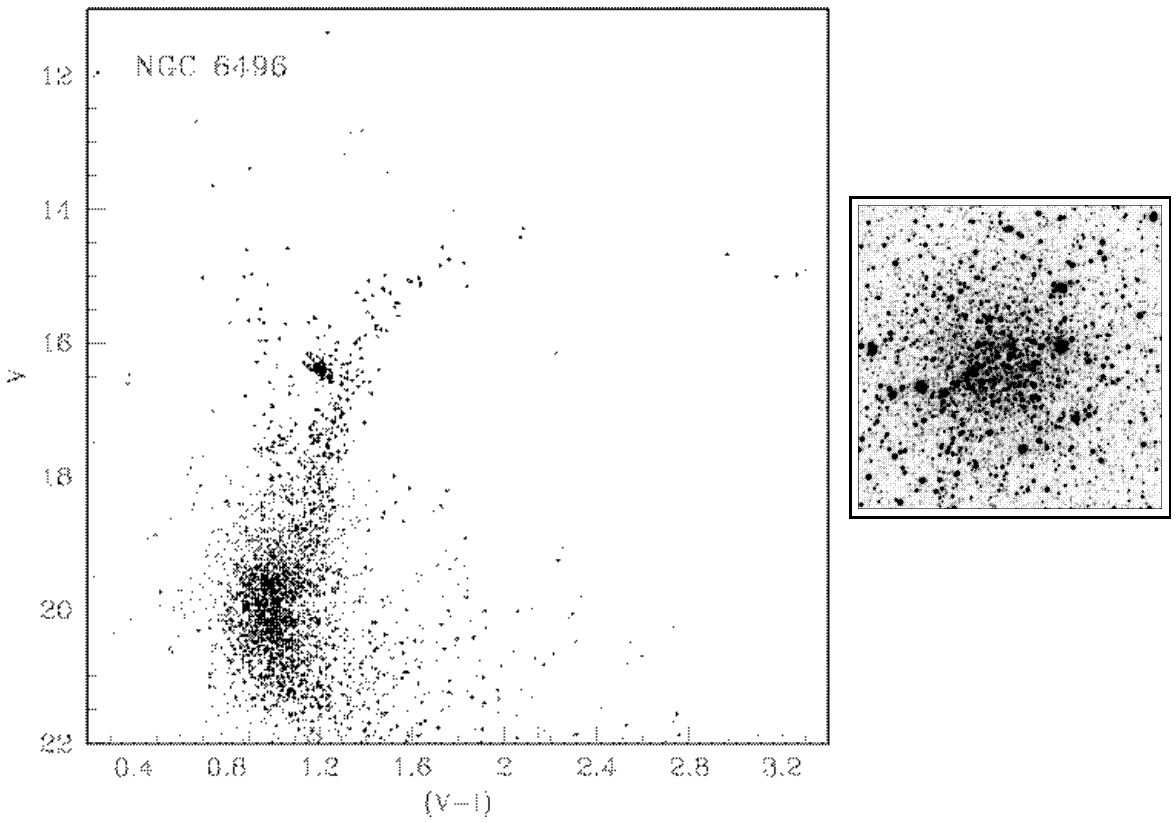

Fig. 30. CMD and covered field for NGC 6496

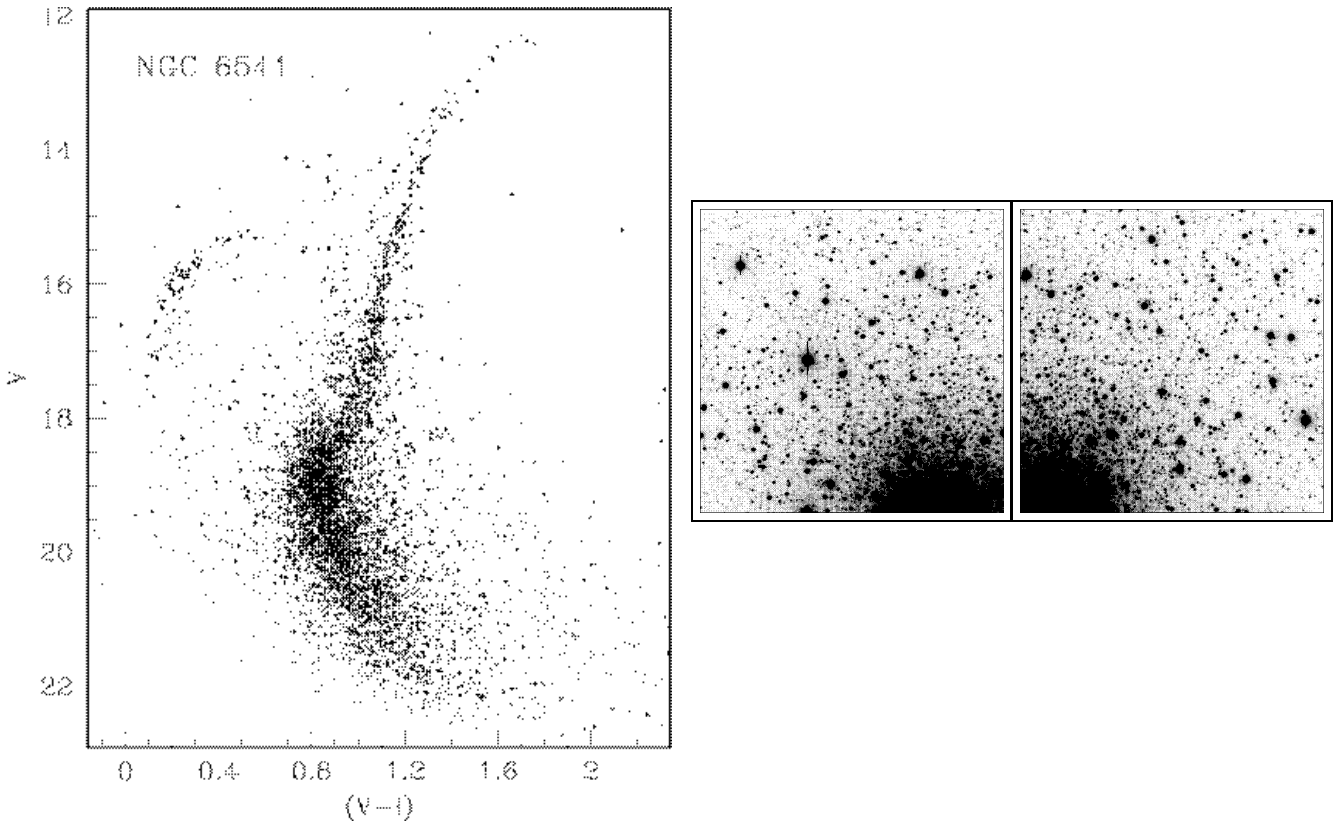

Fig. 31. CMD and covered fields for NGC 6541

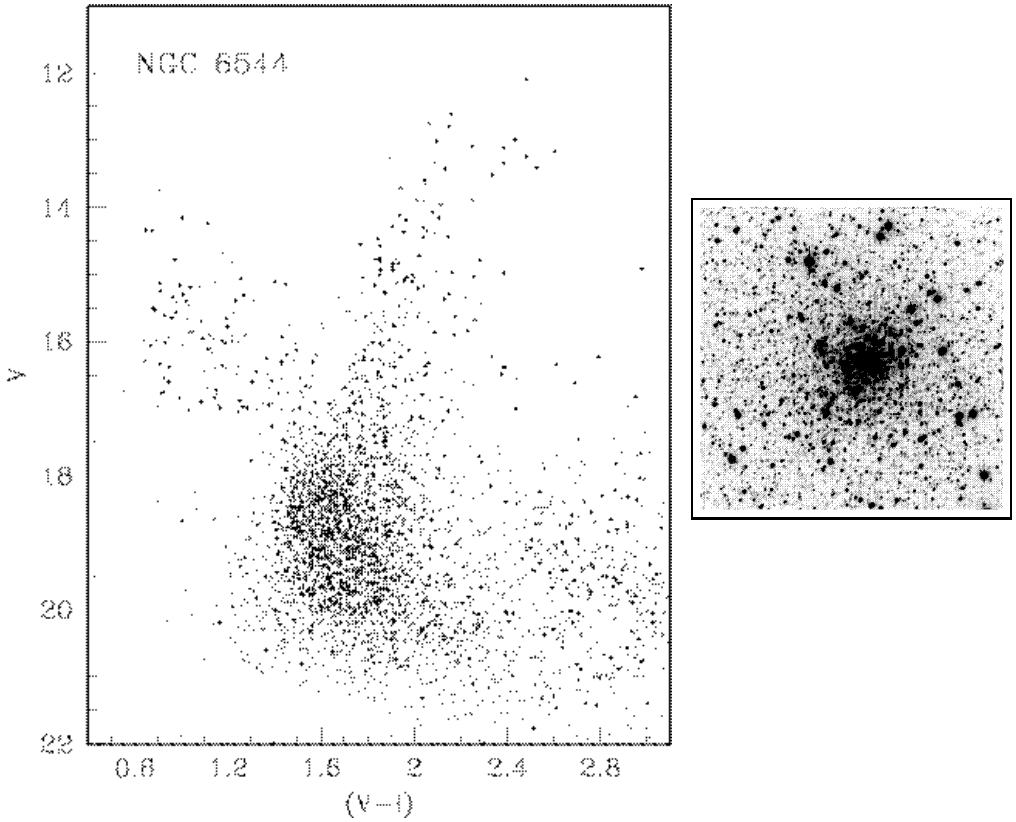

Fig. 32. CMD and covered field for NGC 6544

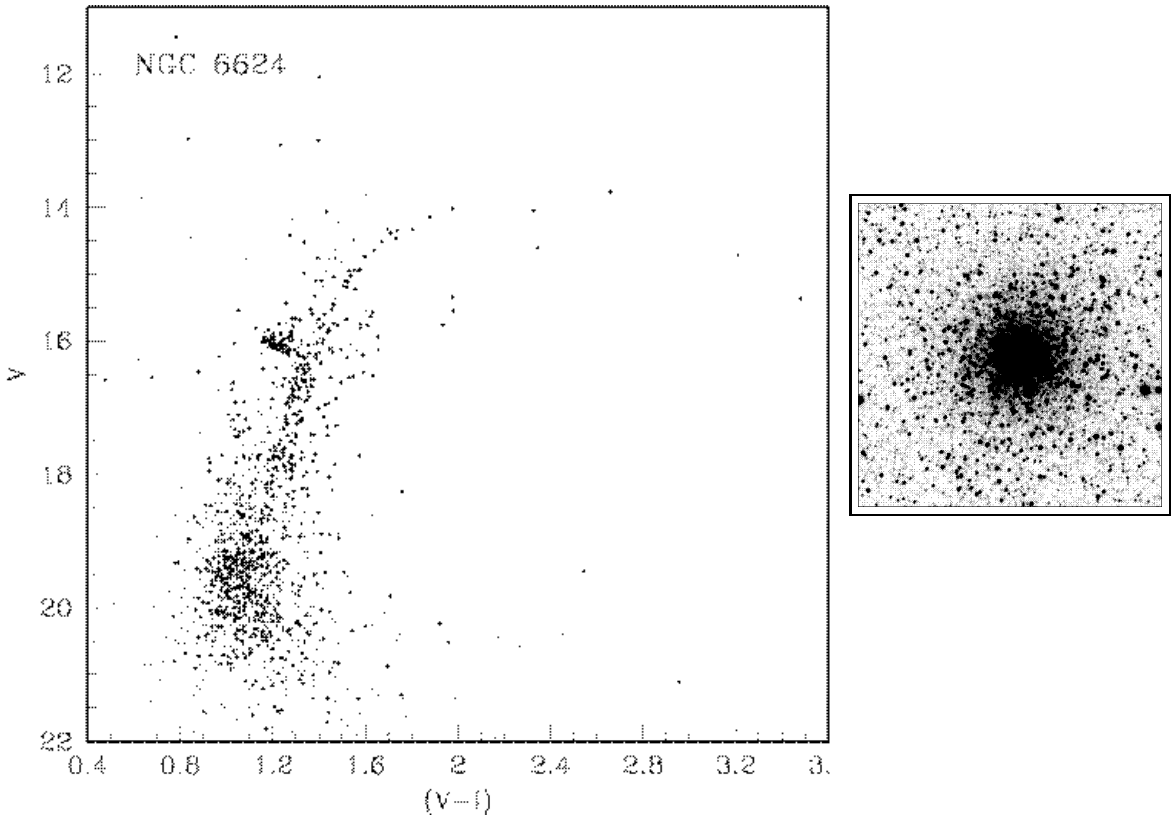

Fig. 33. CMD and covered field for NGC 6624

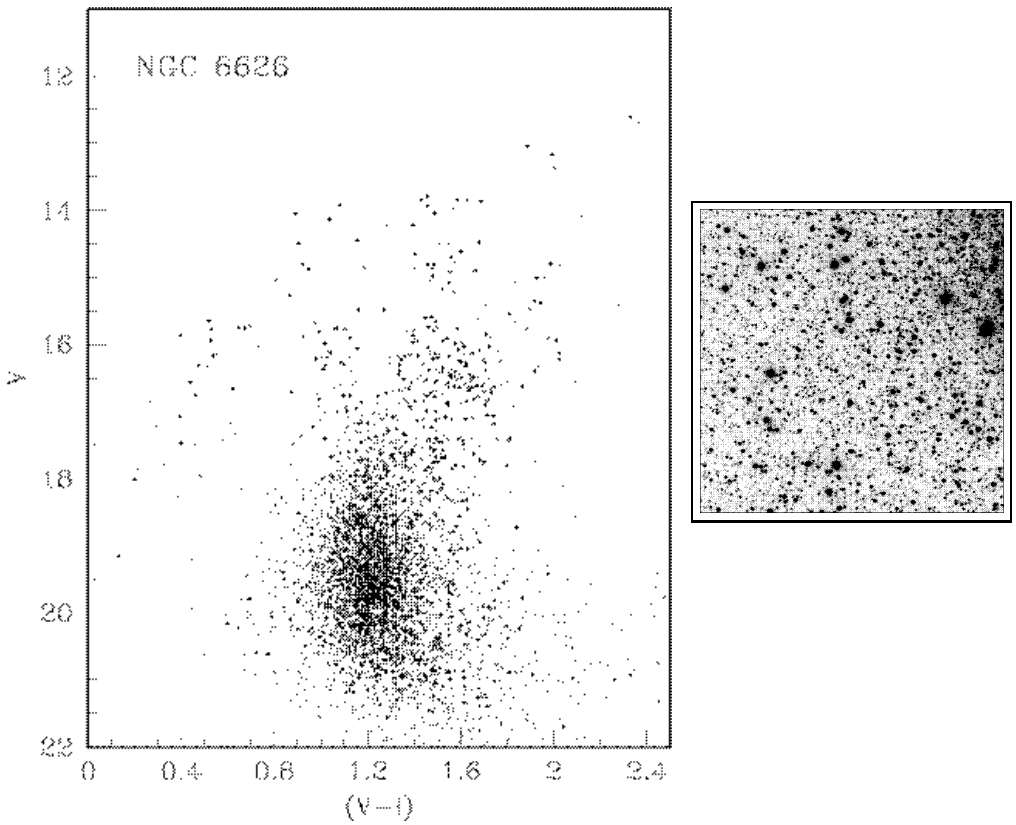

Fig. 34. CMD and covered field for NGC 6626 (M 28)

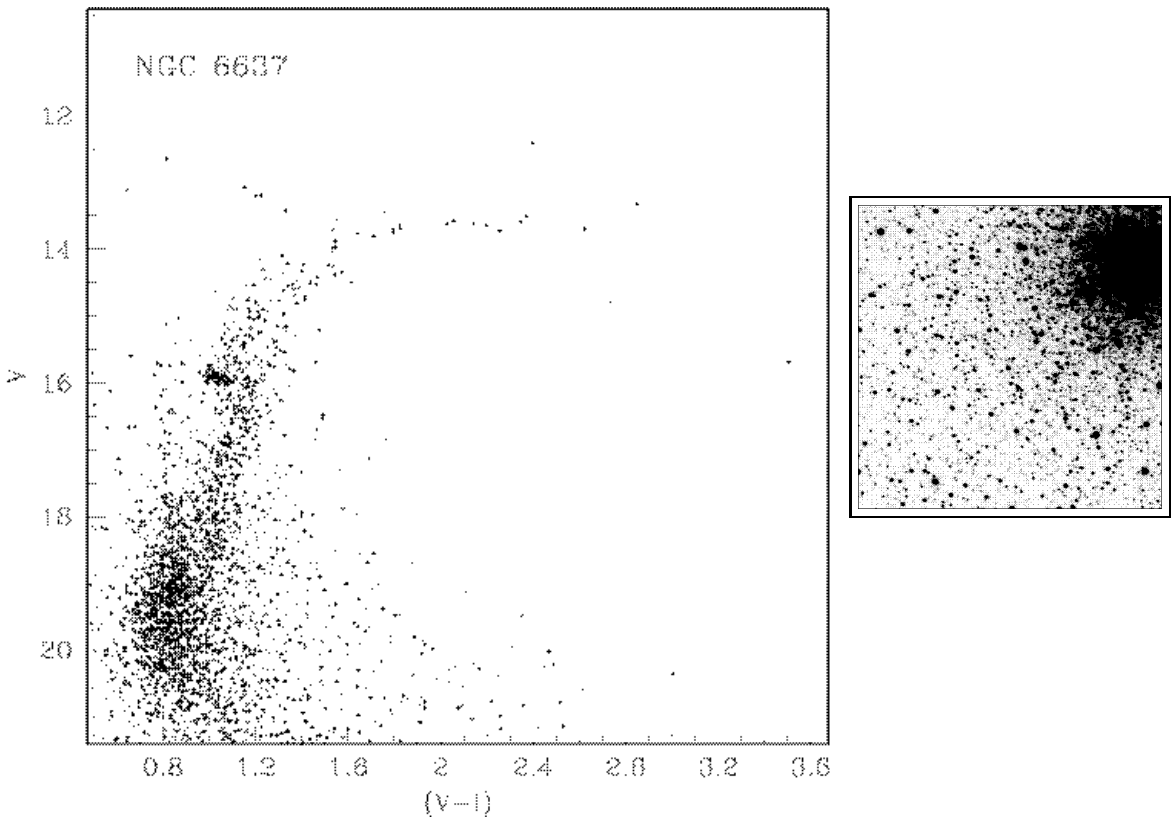

Fig. 35. CMD and covered field for NGC 6637 (M 69)

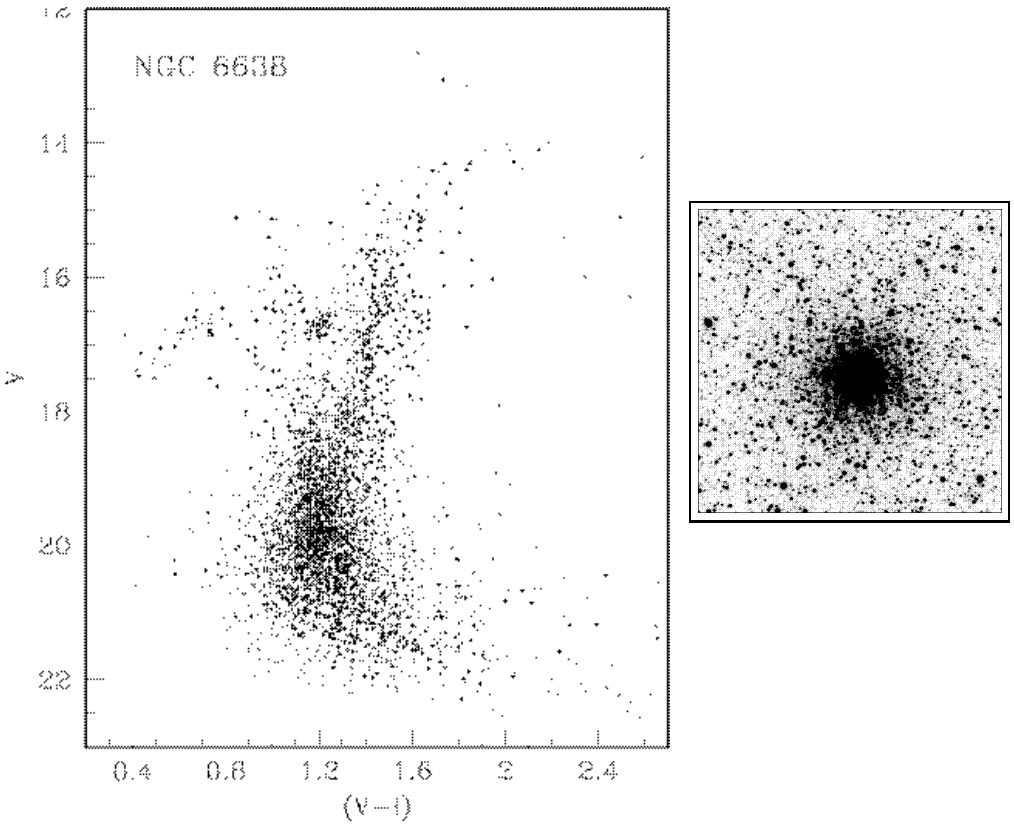

Fig. 36. CMD and covered field for NGC 6638

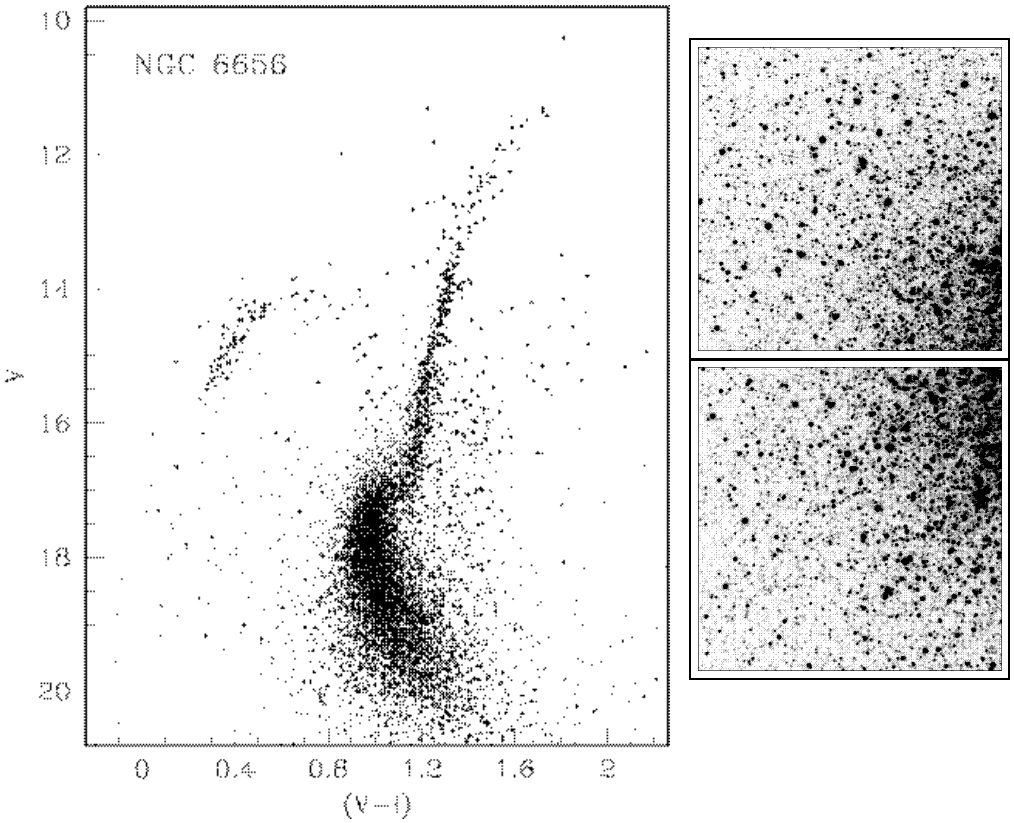

Fig. 37. CMD and covered fields for NGC 6656 (M 22)

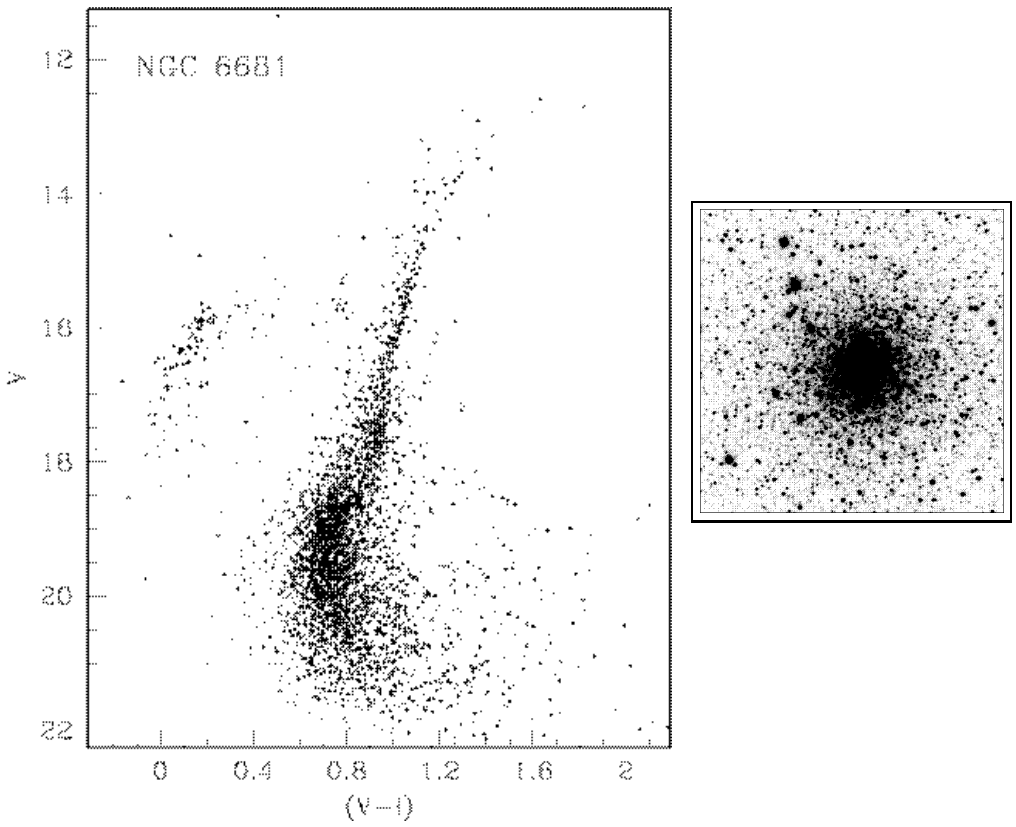

Fig. 38. CMD and covered field for NGC 6681 (M 70)

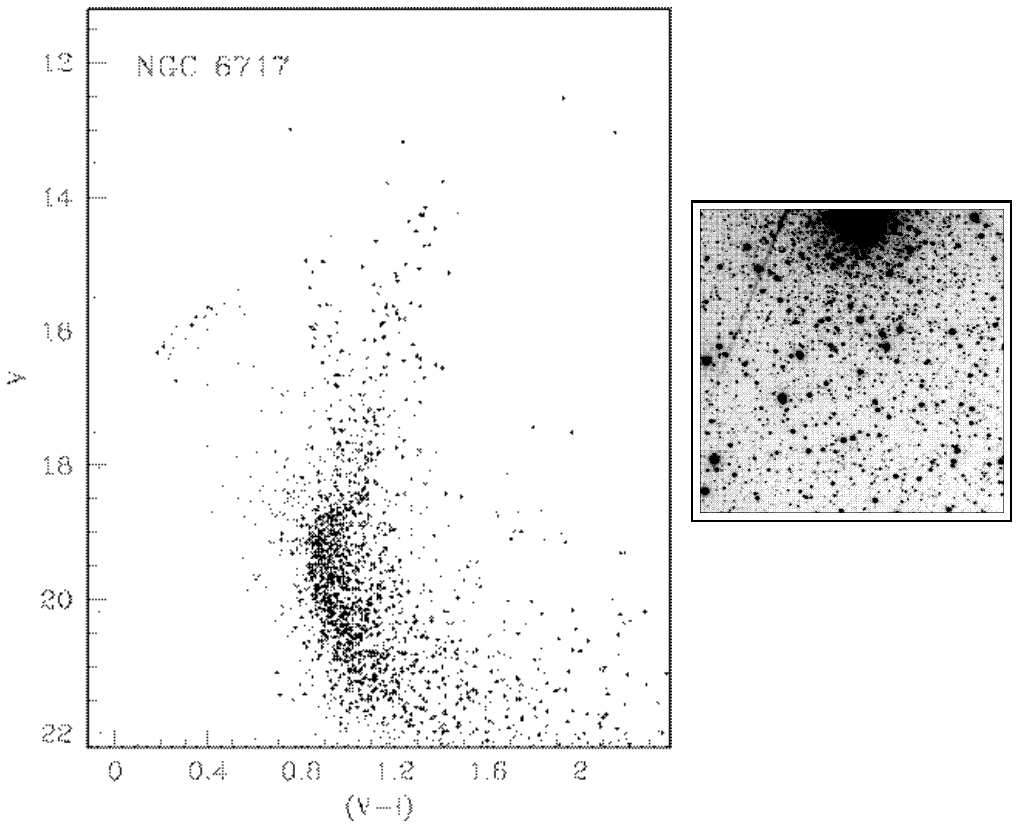

Fig. 39. CMD and covered field for NGC 6717 (Palomar 9)

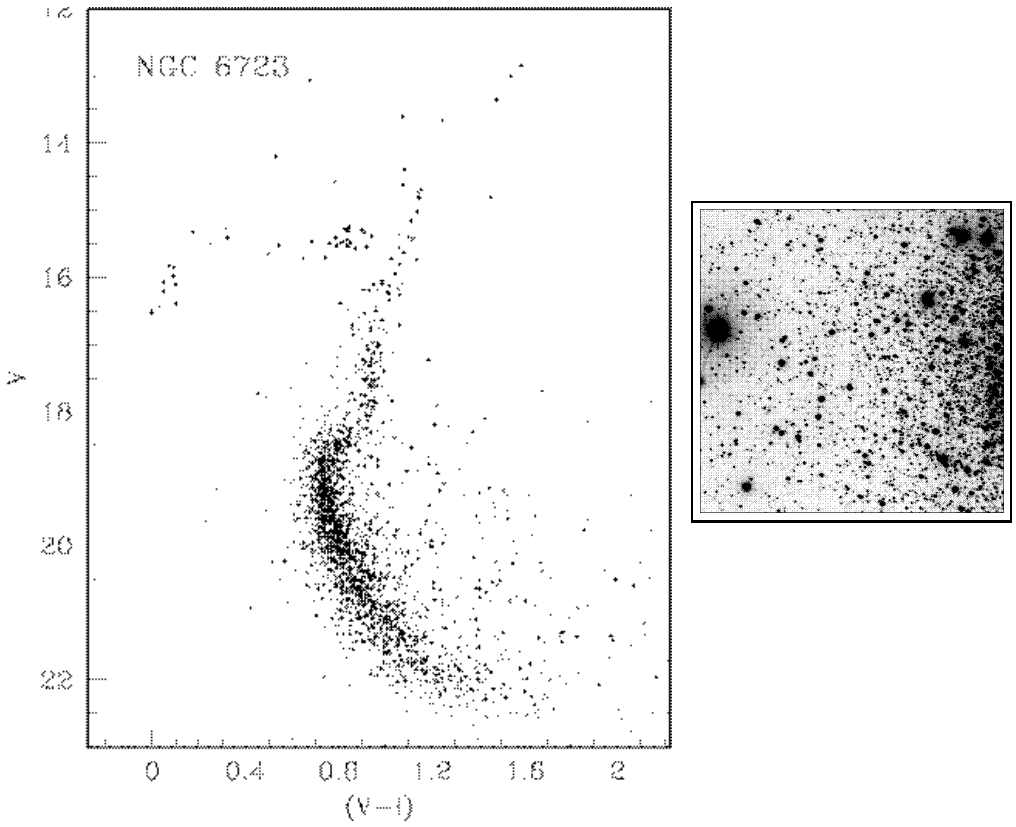

Fig. 40. CMD and covered field for NGC 6723

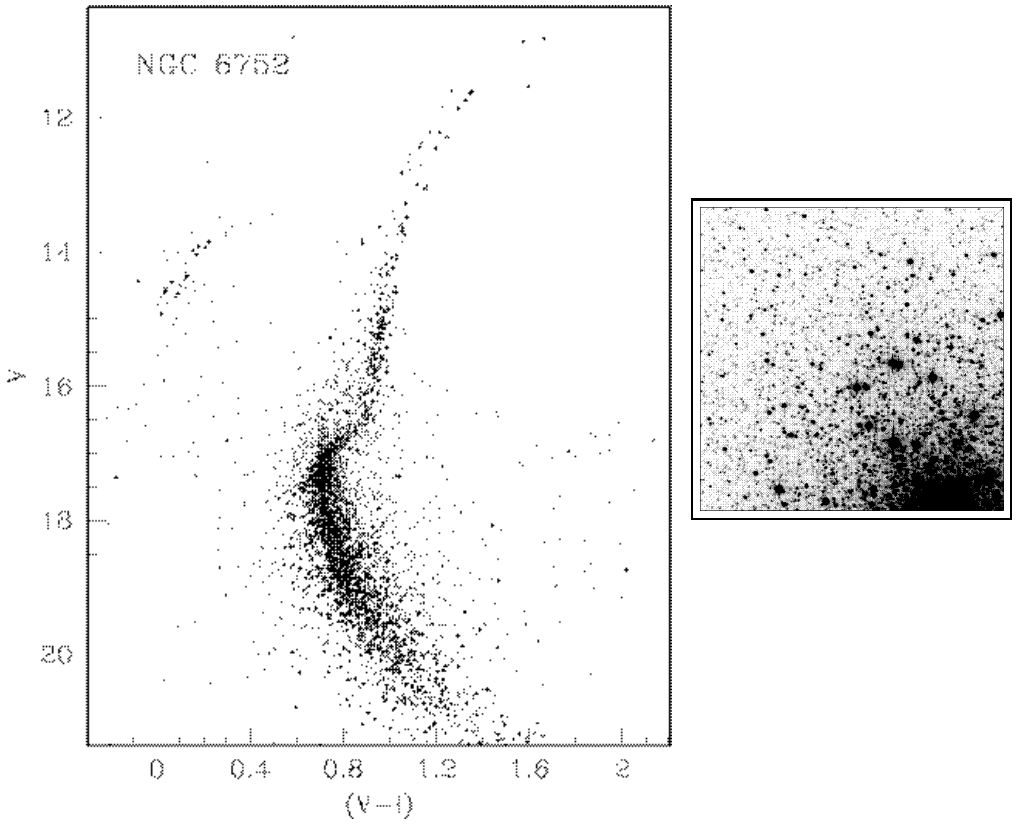

Fig. 41. CMD and covered field for NGC 6752

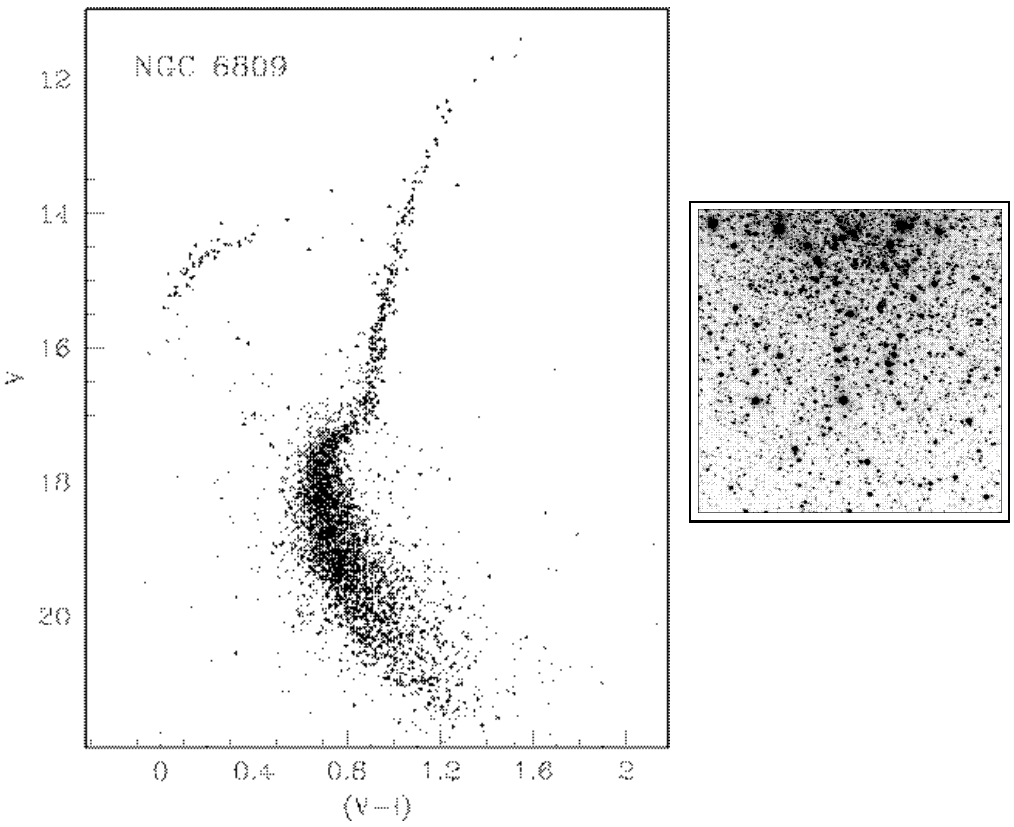

Fig. 42. CMD and covered field for NGC 6809 (M 55)